Treball de Fi de Grau

Grau en Enginyeria en Tecnologies Industrials (GETI)

Development of muscle torque generators for optimal control tracking of human walking

MEMÒRIA

Autor: David Lasierra Hernández

Directors: Míriam Febrer Nafría

Josep Maria Font Llagunes

Convocatòria: Juliol 2022

Escola Tècnica Superior
d'Enginyeria Industrial de Barcelona

Abstract

Muscle torque generators (MTGs) can be used as an alternative of detailed musculoskeletal models in computer simulations of human movement, and have been used by researchers to generate accurate dynamic simulations while mantaining a reasonable degree of biofidelity.

The main goal of this thesis is to improve the reliability of two torque-driven models (*i.e.*, at skeletal level) of different complexity when muscle torque generators are added to them in order to perform a concrete motion. For this purpose, we defined two problems based on different optimal control techniques. The first problem predicts the motion of a simple pendulum model and the second one tracks experimental data from a human walking motion in a 2D HAT (head, arms and trunk) model. In both problems, two versions of the models are considered: a torque-driven version and a version in which muscle torque generators are employed. Both torque-driven models are obtained from the $OpenSim$ repository and the implementation of the MTGs has been programmed with $MATLAB$.

For each problem, different studies were conducted to reach the stated goal. In the predictive problem, several simulations were carried out based on different initial and final conditions. Subsequently, a qualitative evaluation between both models showed that muscle torque generators were slightly advantageous than its torque-driven version when the studied simulation encompassed a shorter range of motion. Conversely, in the tracking problem, a more complex study was performed, based on different optimal control formulations. A final quantitative assessment showed that the tracking in torques was adequate and quite similar between models, but when tracking experimental coordinates the torque-driven version provided better results. Despite the fact the tracking with MTGs was correct, a more realistic behaviour than its torque-driven version was expected.

This project can be considered a first research work in muscle torque generators modelling in the Biomechanical Engineering Lab (BIOMEC) at UPC. Thus, further studies would need to be conducted in order to obtain a more realiable modelling. Parameters such as the maximum isometric torque or the characteristic musculotendon curves involved in the MTGs could be more in depth investigated to gain better insights.

Contents

List of Figures

List of Tables

1 Introduction

1.1 Motivation

The human musculoskeletal system, responsible for the locomotion, is composed by about 200 bones and 300 muscles. The development of models of such a complex system is a non-trivial task that involves the traditional compromise between straightforwardness and accuracy. On the one hand, the models should be complex enough to deliver accurate estimations of the phenomena studied. On the other hand, the models should be simple enough to keep the problem tractable and the results and analysis straightforward [1].

Using detailed musculoskeletal models in computer simulations of human movement can provide insights into individual muscle and joint loading; however, these muscle models increase problem dimensionality and require difficult-to-fit parameters [15]. This prompts the question regarding what methods are available to maintain accuracy within a given musculoskeletal model while limiting the required computational demand. To mitigate these effects while maintaining a reasonable degree of biofidelity, we employ muscle torque generators (MTGs).

The implementation of MTGs in complex models can be tedious at first. However, if the model is simplified from several degrees of freedom to only one, then the problem formulation becomes easier to understand and also an extension of the problem to a more complex version can be easily done. Therefore, in this thesis, two problems of different complexity have been evaluated. In both cases, a torque-driven model and a model which includes MTGs have been studied.

1.2 Project objectives

The main goal of this thesis is to improve the reliability of two torque-driven models of different complexity when muscle torque generators are added to them in order to perform a concrete motion. The first study is based on a predictive optimal control problem that uses a simple pendulum as a model. Whereas the second study is based on an optimal control tracking problem, in which the ability of the model to reliably reproduce a gait cycle is evaluated.

The specific objectives that involve the main goal of this project are:

- Research the state of the art in the modelling of muscle torque generators for human motion simulations.
- Implement muscle torque generators in a simple pendulum model with $MATLAB$.
- Compare the predictive behaviour between the torque-driven model and the MTG-based model through a qualitative evaluation.
- Study different optimal control formulations for human gait tracking when muscle torque generators are taken into account in the model.
- Implement muscle torque generators in a 2D HAT model with $MATLAB$.
- Compare the tracking behaviour between the torque-driven model and the MTG-based model when a quantitative evaluation is conducted.

2 Theoretical background

This section gives theoretical insight into the basis of human walking and its modelling, as well as some key concepts used throughout the project.

2.1 Biomechanics of human motion

2.1.1 Anatomical planes

In order to describe the orientation and location of human body structures it is convenient to define some reference planes (see Figure 1). They are called anatomical planes and they separate the body into different sections. Those are:

- The **sagittal** plane. It splits the human body up into left and right sections.
- The **coronal** plane. It divides the body into posterior and anterior portions.
- The **transverse** plane. It separates the body into an upper and a lower part.

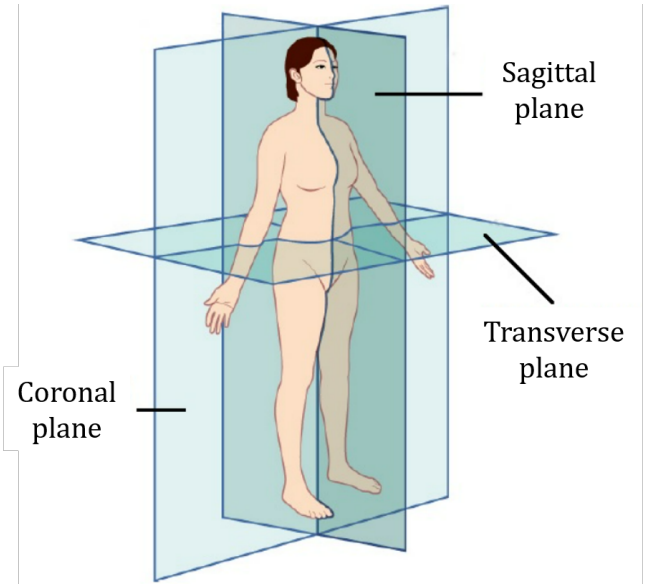

Figure 1: The anatomical planes from the human body. Extracted from [17].

Depending on the type of motion that is analyzed, some planes contain more relevant information than others. Even so, many textbook authors [35] and researchers emphasize in the use of the sagittal plane in gait analysis and ignore the other two. However, when a motion from a pathological subject is analyzed, other planes (*e.g.* the coronal plane in the case of bilateral hip pain) would yield relevant information as well [5].

In this project, a 2D gait model will be used. Only motion in the sagittal plane, which is where most of the movement takes place, will be considered.

2.1.2 Gait cycle

Human walking can be described as a cyclic pattern of body movements which moves forward an individual's position (see Figure 2). Therefore, studying the walking process can be simplified by investigating one walking cycle [2].

Each of these cycles is characterized by a sequence of single and double supports. When one foot is in contact with the ground while the other advances to another support contact, we refer to a single support. Conversely, if both feet are in contact with the ground while the weight is transferred from one limb to the other, then we refer to double support.

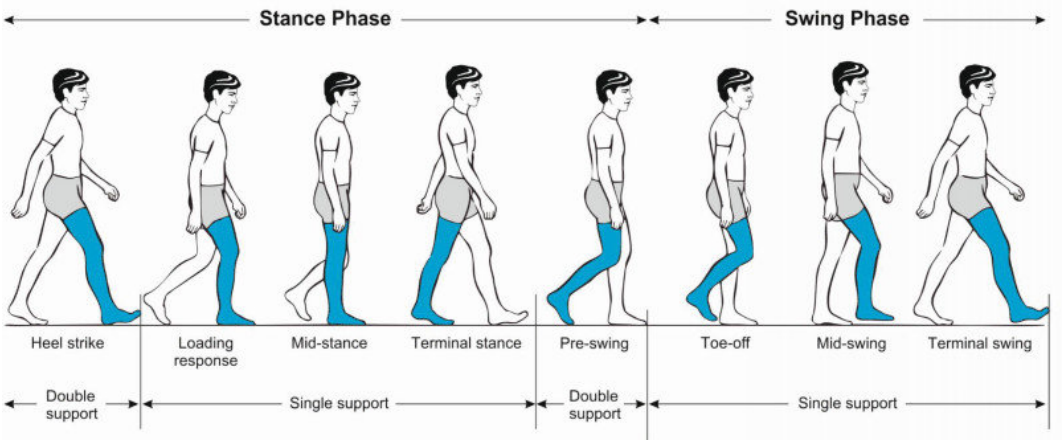

Figure 2: Human walking gait cycle of the right leg. Extracted from [26].

For a single limb, a gait cycle is composed of two phases depending on the period of time when the foot is in contact with the ground. Therefore, we contemplate the stance phase, which is the period of time when the foot is in contact with the ground, and the swing phase in which the same foot is no longer in contact with the ground surface.

Note that Figure 2 shows the human gait cycle from a healthy subject. In this case, the stance phase accounts for 60% of the cycle, whereas the other part corresponds to the swing phase [26].

Another common way to describe the human gait is by the stride and step terms. The step length is the measured distance from the point of foot contact to the point of contralateral foot contact. Hence, two steps make one stride, and thus, the linear distance covered by one gait cycle.

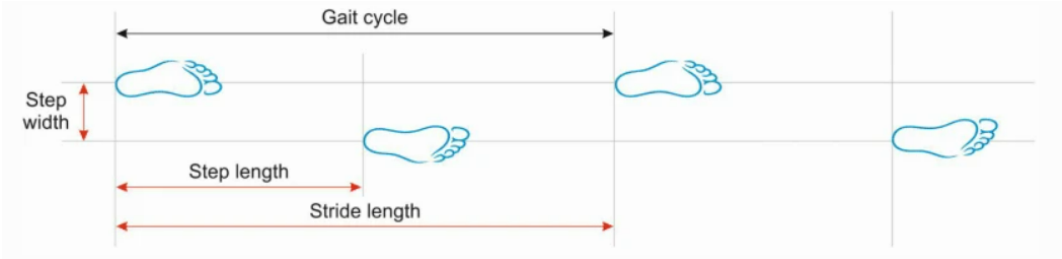

Figure 3: Stride describing the gait cycle. Extracted from [26].

2.2 Multibody system modelling

The human's neuromusculoskeletal system can be viewed as a servo-controlled multibody system in which bones are modelled as rigid bodies connected by joints, actuated by muscles and controlled by the central nervous system (CNS) [11]. These kinds of models are crucial for clinical improvements [12] as well as for the analysis of human motion.

2.2.1 Skeletal modelling

The skeleton is usually modelled as an open kinematic chain which includes rigid segments and joints that link each rigid segment to the next one. These rigid segments represent the bones and they gather physical information such as their actual mass, length, tensor of inertia and center of mass. Those physical variables are called body segment parameters (BSP). The anatomical joints are usually considered as ideal joints and they restrict the relative movement between the bones involved in each joint [1]. Figure 4 shows an example of a biomechanical model which consists of 12 anatomical segments and their corresponding revolute joints which define a 14 degree-of-freedom model.

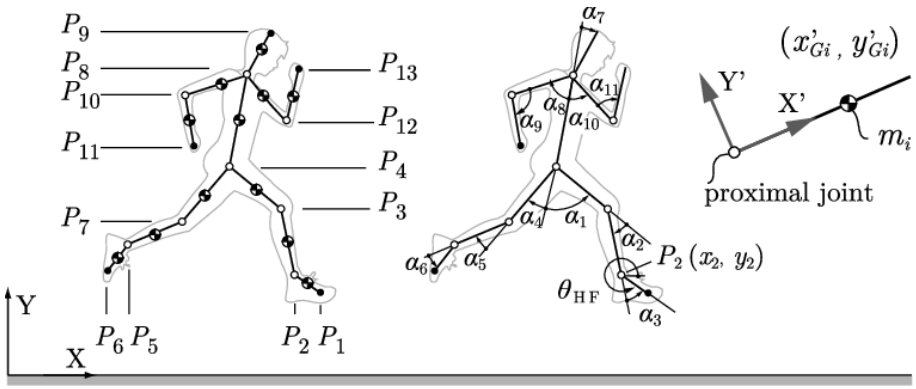

Figure 4: 2D biomechanical model used in a running gait analysis. Extracted from [25].

Depending on the purpose of the study, models can be three- or two-dimensional (as shown in Figure 4), and can represent the whole body or only a part of it [21]. For instance, when a set of bones barely have a relative movement between them, they can be assembled as a single body. That leads to an easier way to tackle complex formulations and thus, can be simplified. A common example in human walking is the so-called HAT model, where head, arms and trunk are modelled as a single body, whereas legs are more precisely modelled. An example of a HAT model is represented in [10].

In this thesis, several models of different complexity will be used in order to determine the equations of motion needed in the dynamic analysis. For this purpose, some analytical expressions such as the Newton-Euler equations or Lagrange equations can be applied. The Newton-Euler method relates the motion of each rigid body with the sum of external forces and torques that act on each element. An example of this formulation can be found in [1]. While the above-mentioned method obtains the motion equations from forces and torques, the Lagrange formulation allows to systematically obtain them from the kinetic and potential energies of the multibody system and the involved generalized forces. An example of this second methodology is shown in [30].

2.2.2 Individual muscle modelling

The mechanical behaviour of muscle tissue can be described by means of passive elements such as springs and damping elements [28]. Commonly, these elements are represented by massless actuators in the model; and their actual mass is considered to be rigidly attached to bones [32]. These elements, combined properly, allow to understand the response of muscle tissue under compressive and tensile loads [28].

In the literature [36] it is possible to find different models that combine the properties of those mechanical components. For instance, the contraction of the muscle-tendon dynamics can be modelled as a pair of muscle torque generators (as it is described in Section 2.2.3), but also as the so-called Hill-type muscle model [14], which is described in this section. See Figure 5 for an illustration of the muscle model.

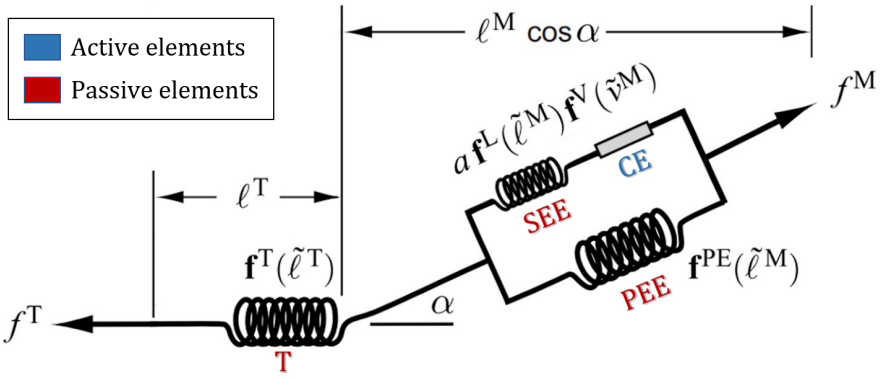

Figure 5: The Hill-type muscle model. Adapted from [9] and [37].

The model consists of four overall components: the contractile element (CE), the serial elastic element (SEE), the parallel elastic element (PEE), and the tendon (T). CE represents the active, *i.e.*, contractile, properties of the muscle, whereas SEE, PEE, and the tendon represent passive nonlinear stiffness. SEE represents the elasticity of the actin-miosyn crossbridges, PEE represents the passive elastic properties of the muscle fibers, and the tendon captures the elastic properties of the tendon and the aponeurosis combined [37]. The contribution of these elements to overall tension can be represented graphically via four characteristic curves [9]:

- The **force active length curve** f_a. It represents the active tension generated by the CE of the sarcomere, that is, the interaction between myofibrils. The peak tension is reached when sarcomeres are at their resting length ℓ^{opt}, as this provides the optimum alignment between the actin and myosin filaments. The function presents a decline in force-generating capacity with shortening and lengthening. That is due to the fact that myofibrils overlap each other when shortening or because they are out of range from each other during the sarcomere lengthening. While in the first case, there is no further potential for myofibrils to contract, the latter means fewer myosin heads binding with actin filaments [27]. In both extreme cases, that leads to no force generation.

- The **passive force length curve** f_{PE}. It shows the passive tension generated by the PEE and therefore it does not contribute to the generation of tension with shortened lengths. As sarcomere lengths increase, the passive tissues reach their full length and start to provide resistance to further increases in length [27]. The length where force starts to rise is called slack length ℓ_0 and it is usually the same as ℓ^{opt}.

- The **force velocity curve** f_v. It describes the fact that the force-generating capacity of the muscle also depends on the contraction velocity and on whether it is an eccentric or concentric contraction. The force-generating capacity of the muscle increases for eccentric contraction, whereas it declines for concentric contraction [37].

- The **tendon force length curve** f_T. The forces generated by CE and PEE are transferred to the bone through the tendon. The tendon is nonlinearly elastic and the force-strain relationship of the tendon includes a slack region, where no force is generated, and nonlinear elasticity when strained that gets gradually more linear at higher strain [37].

Despite the fact that most Hill-type muscle models share the same mathematical formulation, these characteristic curves may differ between models by changing some of the parameters that define them. Figure 6 illustrates the characteristic curves for the *Thelen2003* [33] and the *Millard2012* [7] models together so that the differences between these curves can be clearly seen.

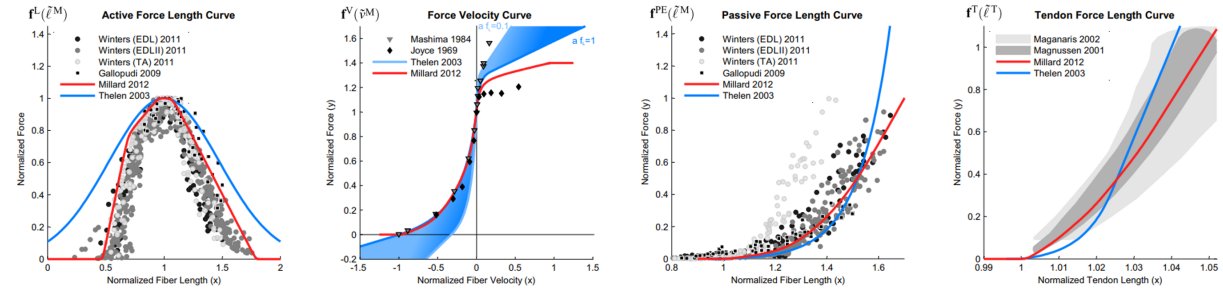

Figure 6: The characteristic musculotendon curves. Extracted from [9].

2.2.3 Muscle torque generators

Any movement in the body is the result of the coordination of action between agonist and antagonist muscles. That means that when a muscle contracts to produce a movement (agonist), the other is relaxed to allow the motion to occur (antagonist). For instance, when a bicep curl is performed (Figure 7a), the biceps will be the agonist as it contracts and raises the forearm, whereas the triceps will be the antagonist since it relaxes. Figure 7b shows the opposite situation.

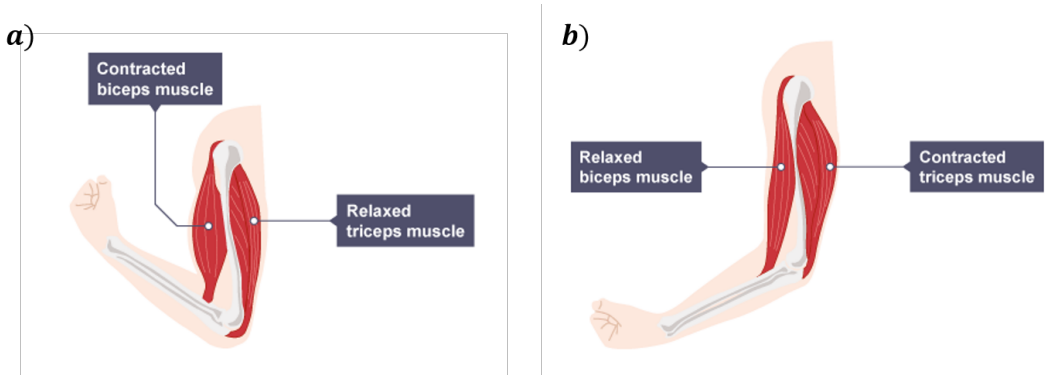

Figure 7: Biceps and triceps as an example of antagonistic pairs. Adapted from [3].

Bearing in mind the non-trivial behaviour of the muscle contraction and the complex geometry which imply when modelling, one method that can simplify the problem while maintaining a reasonable degree of biofidelity is the use of muscle torque generators (MTGs).

Functionally, an MTG provides a joint torque that mimics the behaviour of muscles crossing a given joint [15]. That means that a pair of torques acts at each joint of the model in order to copy the behaviour of agonist and antagonist muscles.

Besides, MTGs also allow multibody system reduction by approximating the characteristic musculotendon curves directly at the joint level. As an example, Figure 8 illustrates a schematic of the knee, ankle, and hip joint within Norman-Gerum's sit-to-stand model [23], actuated by Hill-type muscles (Figure 8a) and actuated by muscle torque generators (Figure 8b):

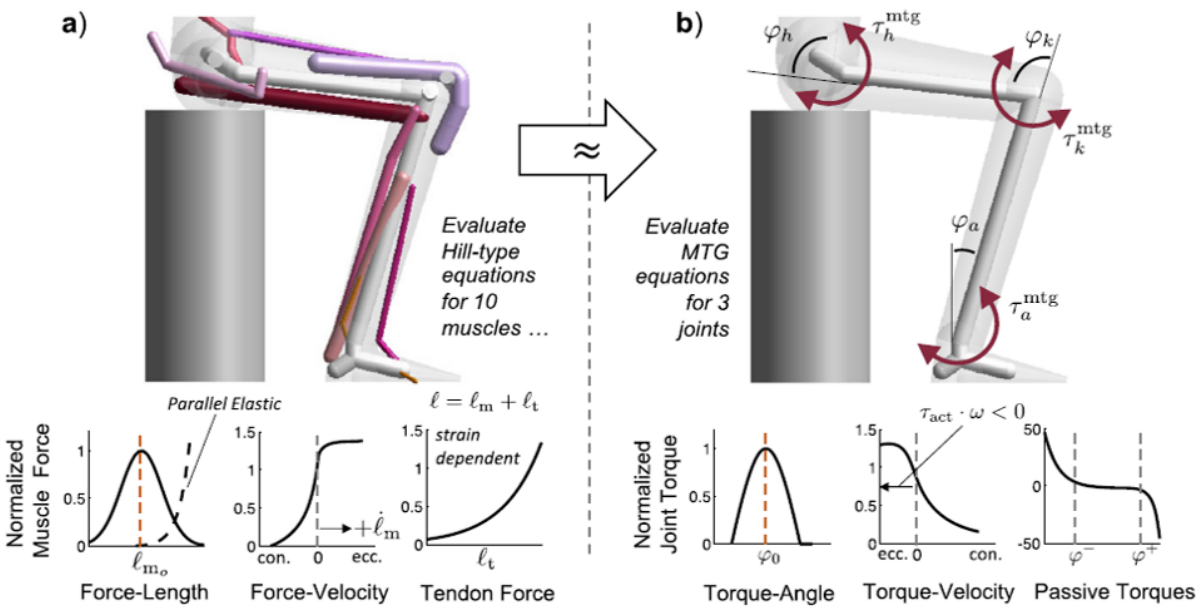

Figure 8: Model actuated by (a) Hill-type muscles and (b) MTGs. Extracted from [15].

In practice, MTG's models can be employed for different purposes. For instance, in [15], three specific cases of MTG-driven multibody sports simulations have been carried out. Other examples are [19], where a set of MTGs have been applied in a wearable robotic system developed to prevent injury to the low back, or in [31], where the MTGs have been implemented in the prediction of a pathological gait.

In this thesis we employ muscle torque generators in models of different complexity in order to improve the reliability of their respective model at skeletal level when performing a concrete motion.

2.2.4 Foot-ground contact modelling

A foot-ground contact model determines the interaction between body and ground. Regarding the modelling of foot-ground contact interaction during walking, there are mainly two options: using kinematic constraints (hard contact) or a constitutive contact model (compliant contact) [20].

The first approach defines the interaction between the foot and the ground using ideal kinematic constraints, which change at each phase of the gait cycle [20]. Therefore, foot can be modelled as a rigid body and hence, numerical stiffness of the model does not change from swing to stance phase [6] (see Figure 9a).

Conversely, the second method establishes a physical relationship between the developed contact forces (normal and tangential) and the relative foot-ground displacements and velocities [20]. Viscoelastic models such as in [18], or volumetric contact models like in [4] (see Figure 9b), are adequate approaches for this method.

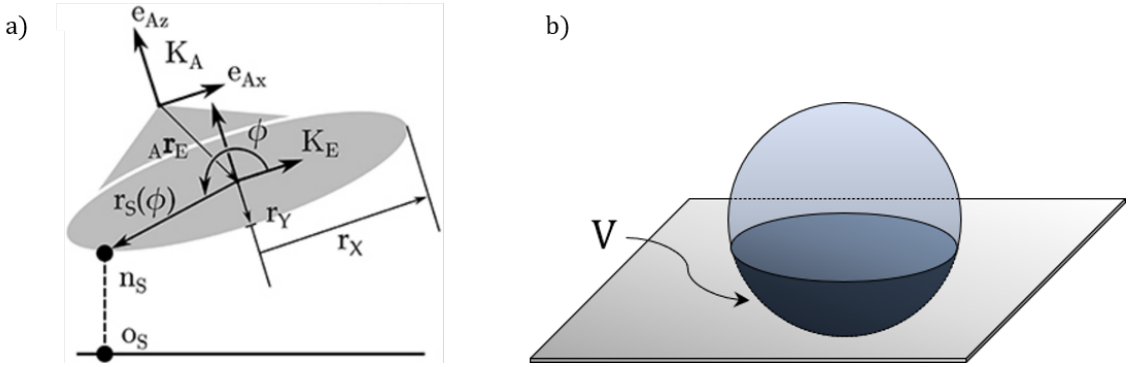

Figure 9: Foot-ground contact modelled as (a) a kinematic constraint between an ellipse and a plane (extracted from [18]) and (b) a constitutive volumetric contact model.

In this thesis, no contact model has been used since the gait problem studied is based on tracking experimental data and therefore the experimental forces are imposed as the ground reaction forces (GRF) of the model.

2.3 Dynamics Analysis

Once the model is obtained, a dynamic analysis is carried out to better understand how the motion of study is performed. For example, a dynamic analysis can be useful to determine muscle forces, to analyse the way the central nervous system controls a motion, or to compare a healthy motion against an impaired one [21].

Depending on the purpose of the study, two kinds of dynamic analyses can be carried out: the inverse dynamic analysis (IDA) or the forward dynamic analysis (FDA).

2.3.1 Inverse Dynamic Analysis

Inverse dynamic analysis consists in obtaining the net joint torques involved during the motion of study. These torques can be obtained from kinematic data, ground reaction forces (GRF) and the physical characteristics from the model (the body segment parameters).

Mathematically speaking, this approach requires the system's coordinates and its derivatives. Therefore, by evaluating them in the motion equations for a time range, joint forces and torques can be computed.

Reflective markers and force plates are used to obtain motion data and GRF respectively. Since these devices do not provide directly the coordinates nor their time derivatives, a preprocess called inverse kinematics (IK) must be applied (see Figure 10). This consists in solving an optimization problem where the difference between captured marker trajectories and model marker trajectories is minimized.

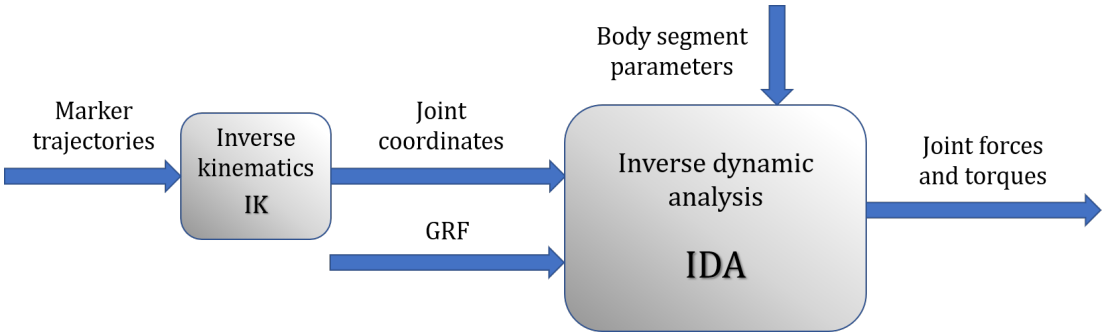

Figure 10: Diagram of an inverse dynamic analysis.

2.3.2 Forward Dynamic Analysis

Forward dynamic analysis describes the motion of the system when some particular forces or torques are applied. The input data in this approach are the muscle forces or the resultant joint torques. Body segment parameters and GRF are considered as inputs as well (see Figure 11). It is also possible to find muscle excitations as input data. In that case, the simulation is called muscle-driven simulation.

Unlike the IDA, in FDA the differential equations of motion shall be integrated with respect to time in order to find the evolution of joint coordinates. This can sometimes lead to integration errors and thus, combined with the unstable character of human walking, conduct to non-stable solutions. However, these errors can be compensated with the use of control methodologies.

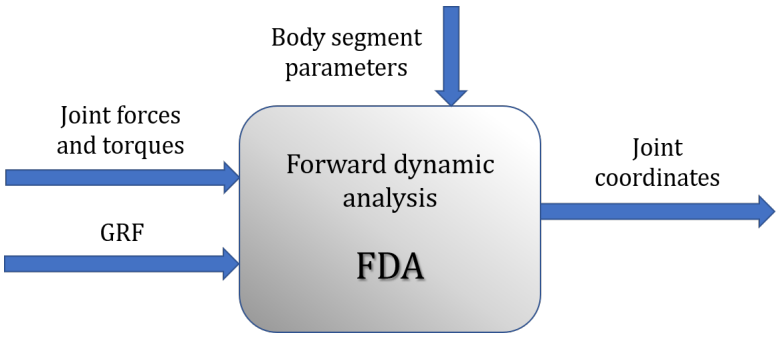

Figure 11: Diagram of a forward dynamic analysis.

In this thesis, an inverse dynamic analysis is carried out within an optimal control formulation. This formulation is explained in the following section 2.4.

2.4 Optimal control prediction

Techniques defined in the previous section 2.3 can be used to predict novel human motions (a priori unknown) for which no experimental data are available at first. During the last years, there has been a growing interest in motion prediction due to its applications. Some of them are: anticipating the result of a surgery, designing assistive devices or analysing the dynamic simulation of a specific motion [24].

There are several ways to predict human motion. However, the most accepted approach consists of formulating an optimisation problem. The main idea is to find which system configuration provides an optimal solution to a problem given some constraints and a cost function to be optimized. Therefore, any optimal control problem is usually defined by the following parameters:

- **State variables**. They are used to describe the current state (position, velocity) of the system. Examples of state variables in gait simulations are: joint coordinates, velocities, muscle length...
- **Control variables**. These variables manipulate the state variables in order to satisfy some desired conditions. Examples of control variables in gait simulations are: joint accelerations, muscle activation/excitation, muscle torques...
- **Dynamic constraints**. They are a set of equations governed in the states and have to be satisfied during the optimization problem.
- **Path constraints**. They are inequalities that must be satisfied during an entire time interval. These restrictions can either be bounds on states and controls, or algebraic path constraints.
- **Boundary conditions** on state and time. Some state and time situations are imposed at the beginning and at the end of the time interval.
- **Cost function**. It is the mathematical expression that wants to be optimized, which is a function of state and control variables.

Different cost functions have been used to predict gait. Some examples are minimizing weighted normalized torques [29] or joint accelerations as well as minimizing muscle activations [13].

In this thesis, we employ optimal control within an inverse dynamic analysis in the problem formulation. The two problems studied in this project (see sections 3.1.2 and 3.2.2) have a similar structure in terms of the problem formulation. However, the first one predicts a novel motion and the other tracks a motion from experimental data. The main difference in these two kinds of formulation lies in the cost function.

3 Methods

This section introduces the models used throughout the project as well as how the muscle torque generators have been implemented in each of them. The implementation of MTGs in complex models can be tedious at first. If the model is simplified from several degrees of freedom to only one, then the problem formulation becomes easier to understand. Not only is it easier to implement the MTGs, but also an extension of the problem to a more complex version can be easily done.

In order to ease the understanding of MTGs in human walking simulations, a simpler problem has been defined. Thus, it was considered that the formulation of a simple pendulum with a single joint could be easily transferred to several joints of the human body. Hence, the chapter is divided into two different parts. The first part corresponds to an optimal control predictive problem using a simple pendulum model, while the second one is an optimal control tracking problem using a 2D HAT model. That means that in the simple pendulum problem we look for a new motion and in the 2D HAT problem we look for a motion which is as close as possible to an experimentally measured one.

In each of the parts two different models are presented: a torque-driven model (*i.e.*, at skeletal level) and a model where muscle torque generators have been implemented. In both problems, the torque-driven model is obtained from the OpenSim repository and the implementation of the MTGs has been programmed with MATLAB.

3.1 Simple pendulum simulations

The simple pendulum problem consists of an $m = 1\ kg$ massive bob which is attached to a massless stick with length $\ell = 0.5\ m$ and they both swing back and forth in a periodic motion. The joint where the motion is produced is fixed to the ground and hence, only rotational motion is allowed. The coordinate that describes this one-degree-of-freedom problem is the angle q and it will change from an initial position q_{ini} to a final one q_{fin} within a bounded time $t \in [t_{ini}, t_{fin}]$. The motion of the pendulum in the torque-driven problem is given by an external moment M_z (see Figure 12a), while in the problem with MTGs, it is due to two torques (see Figure 12b), one associated with the extension τ^{ME} and the other referred to flexion τ^{MF}.

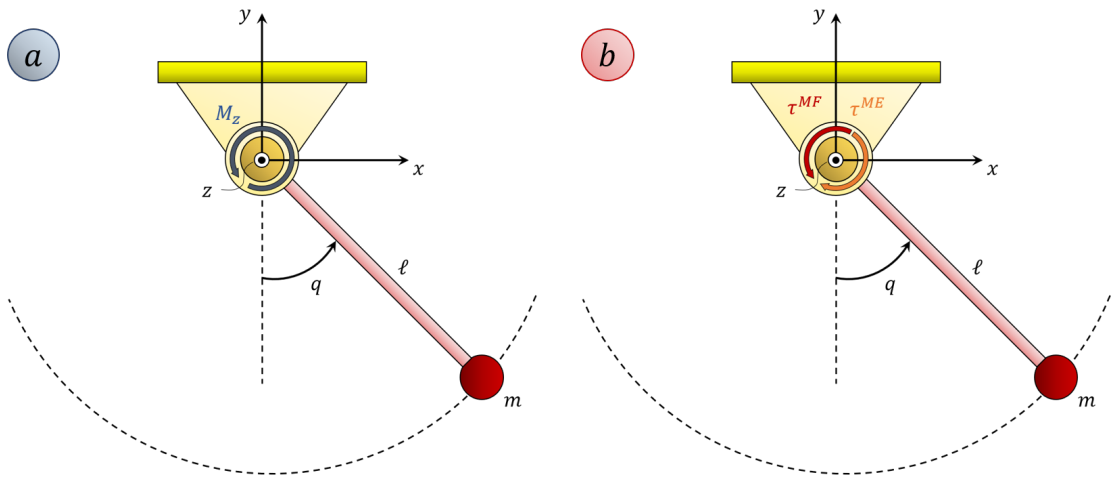

Figure 12: Simple pendulum configuration as a (a) torque-driven model (b) MTGs-based model.

3.1.1 MTGs modelling

The net torque at the model's joint is the sum of the signed flexor and extensor muscle torques acting at that joint:

$$\tau = \tau^{MF} + \tau^{ME} \tag{1}$$

Since each muscle torque acts in a single direction, there are two MTGs acting at the joint, a flexor τ^{MF} and an extensor τ^{ME}. The torque τ^{M} developed by a single MTG is given by an adapted formulation from [19]:

$$\tau^{M} = \tau_o^{M} a \mathbf{f}^{A}(q)\, \mathbf{f}^{V}(\dot{q}) \tag{2}$$

The torque developed by Equation 2 is a function of the control input a from the solver, the angle q, and the angular velocity $\dot{q}$ of the joint. While the angle of the joint changes the value of the passive torque-angle curve $\mathbf{f}^{A}(q)$, the angular velocity of the joint affects the value of the torque velocity curve $\mathbf{f}^{V}(\dot{q})$. Finally, the parameter τ_o helps to build the characteristic curve of the MTG as it provides the maximum value achieved during the motion. Either the flexor and extensor maximum torques were set to $\tau_o^{MF} = \tau_o^{ME} = 10\, Nm$. These values were adjusted from the torque-driven problem.

In this model, the characteristic curve $\mathbf{f}^{A}(q)$ was defined as a parabolic function as it follows:

$$\mathbf{f}^{A}(q) = \frac{1}{4p} \cdot q^2 - \frac{h}{2p} \cdot q + \frac{h^2 + 4pk}{4p} \tag{3}$$

where (h, k) correspond to the vertex coordinates and p changes the concavity of the function. These parameters were set as: $h = -0.02\ rad$, $k = 1$ and $p = -0.57\ rad^2$.

Conversely, the torque velocity curve $\mathbf{f}^{V}(\dot{q})$ was extracted from the literature [28] and can be written as the following piecewise function:

$$\mathbf{f}^{V}(\dot{q}) = \begin{cases} 0 & \text{for} \quad \dot{q} \leq -1, \\ \frac{1+\frac{\dot{q}}{k_{CE1}}}{1-\frac{\dot{q}}{k_{CE1}}} & \text{for} \quad -1 \leq \dot{q} \leq 0, \\ \frac{1+\frac{\dot{q} f_{max}}{k_{CE2}}}{1+\frac{\dot{q}}{k_{CE2}}} & \text{for} \quad \dot{q} > 0 \end{cases} \tag{4}$$

where k_{CE1} and k_{CE2} are force velocity shape factors and are set to $k_{CE1} = 0.25$ and $k_{CE2} = 0.06$ in this work. In contrast, f_{max} is the maximum normalized achievable torque and it is set to $f_{max} = 1.6$.

3.1.2 Optimal control predictive problem

To predict the simple pendulum motion, two different models have been used: the torque-driven model and the MTG-based model. Therefore, the formulation of the problem differs depending on which model is studied. Table 1 shows the optimal control configuration for each of the models, where all the magnitudes are represented in the international system units.

Both problems have the same state variables and the angular coordinate q will move from an initial position q_{ini} to a final one q_{fin} within a bounded time $t \in [t_{ini}, t_{fin}]$.

Note that a reserve actuator $\tau_{reserve}$ was added in the controls from the MTG-driven statement. This torque will help to satisfy the path constraints when the MTG torques are unable to perform the desired motion. Also, note that the activations are only considered in the MTG-driven statement since they are only dependant on the muscles. As it is stated in section 2.4, these activations together with M_z as well as $\tau_{reserve}$ will be considered in the cost function to minimise.

It is also remarkable that the path constraints are different for each model. While in the torque-driven model the generated torque at the joint has to be equal to the one computed with the inverse dynamic analysis, in the MTG-driven is the sum of the flexor and extensor muscle torques (plus the reserve actuator).

Table 1: Simple pendulum optimal control predictive statement.

	Torque-driven	**MTG-driven**
States	q,$\dot{q}$	q,$\dot{q}$
State constraints	$-\frac{\pi}{2} \leq q \leq \frac{\pi}{2}$	$-\frac{\pi}{2} \leq q \leq \frac{\pi}{2}$
	$-100 \leq \dot{q} \leq 100$	$-100 \leq \dot{q} \leq 100$
Controls	$\ddot{q}, M_z$	$\ddot{q}, \tau_{reserve}, a$
Control constraints	$-100 \leq \ddot{q} \leq 100$	$-100 \leq \ddot{q} \leq 100$
	$-10 \leq M_z \leq 10$	$-10 \leq \tau_{reserve} \leq 10$
		$0 \leq a \leq 1$
Path constraints	$\tau = M_z$	$\tau = \tau^{MF} + \tau^{ME} + \tau_{reserve}$
Cost function	$J = 0.1\tau^2 + 0.01\ddot{q}^2$	$J = 0.1\tau^2 + a^2 + \tau_{reserve}^2$

In order to implement the optimal control algorithm, we used $GPOPS-II$, which works within a $MATLAB$ environment.

3.1.3 Simulations of interest

For each of the two models, four different simulations have been carried out based on different initial and final conditions (see Figure 13). The main purpose of these has been twofold. On the one hand, we wanted to check the consistency of the MTGs for each simulation. For this purpose, the evolution of the system states $(q, \dot{q})$ as well as the M_z torque will be qualitatively compared in both models. On the other hand, a study will also be made comparing the four simulations in which the MTGs have been implemented. In this way, it will be possible to check if the pendulum shows any kind of tendency in its motion depending on its initial and final conditions when the MTGs are applied.

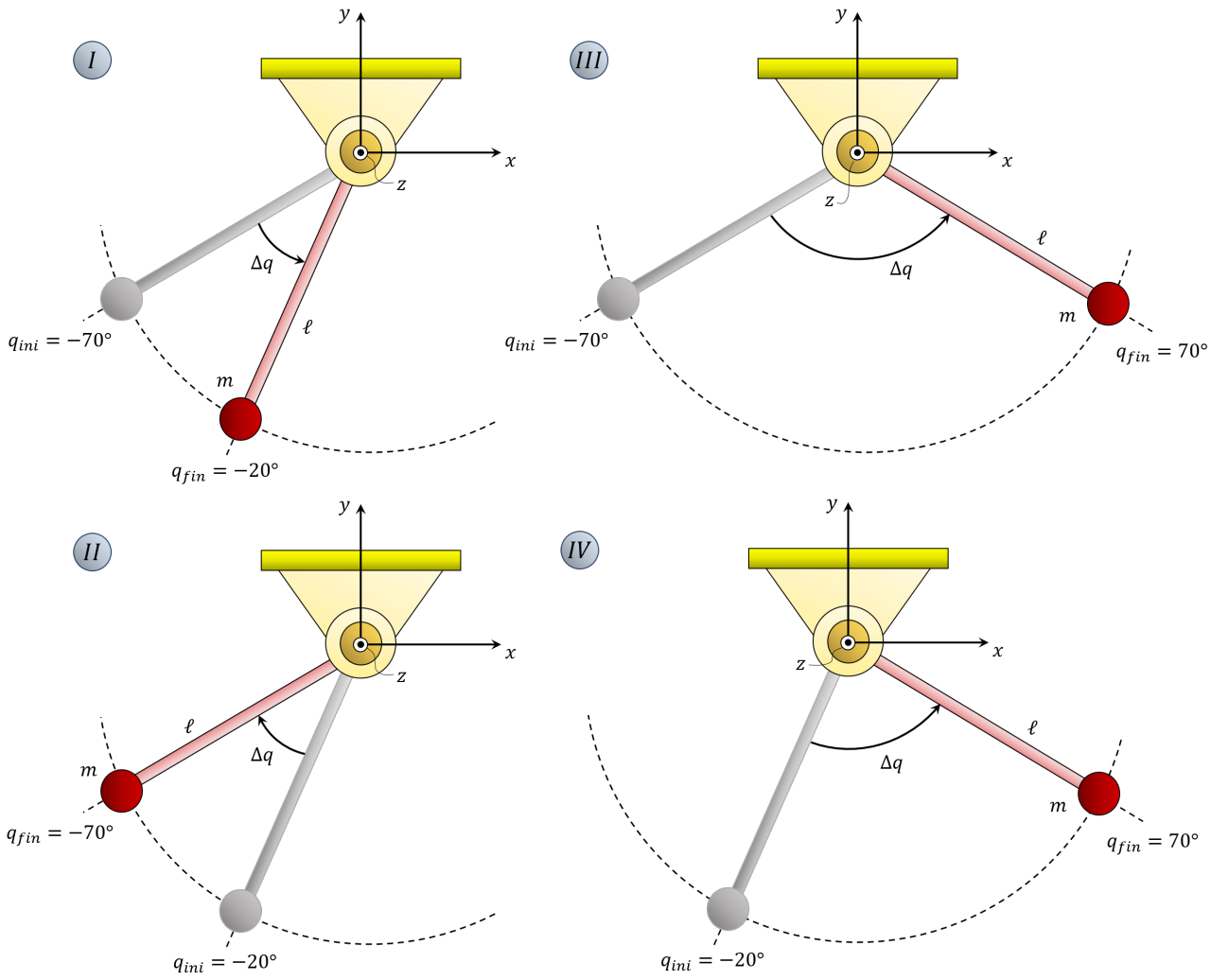

Figure 13: Simple pendulum simulations.

Note that each of the simulations has been conducted in both the torque-driven version and the version with muscle torque generators implemented.

3.2 2D HAT simulations

Having studied the simple case for a single joint as was the case of the pendulum, we can now proceed to a more complex study, which will include several joints as is the case of human walking. Bodies and generalized coordinates of the model are illustrated in Figure 14.

The studied problem consists of ten degrees of freedom (see Table 2). From these ten, the three involving the pelvis are actuated by residual forces and moments. These have been artificially added so that the equations of motion of the system are dynamically consistent.

Table 2: Coordinates and DoF.

Coordinate	Degree of freedom (DoF)
x_0	Pelvis x displacement
y_0	Pelvis y displacement
q_0	Pelvis tilt
q_1	Lumbar extension
q_2	Right hip flexion angle
q_3	Right knee angle
q_4	Right ankle angle
q_5	Left hip flexion angle
q_6	Left knee angle
q_7	Left ankle angle

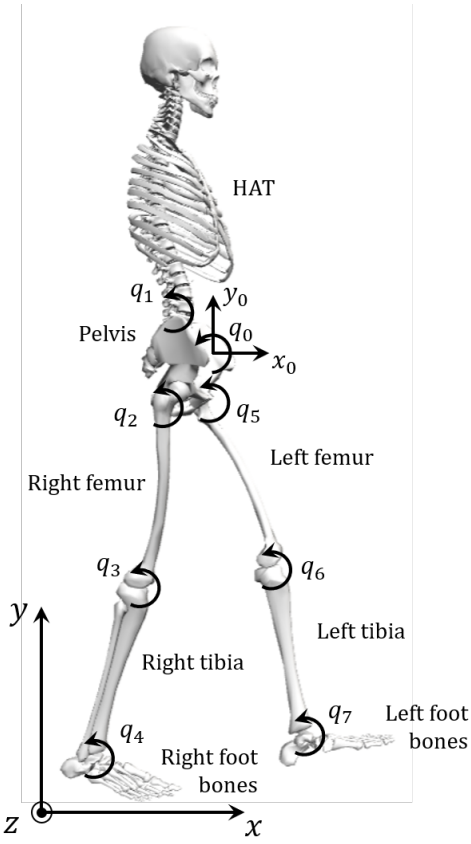

Figure 14: Bodies and generalized coordinates of the model.

The approach that has been studied in this part of the project is to add muscle torque generators on the OpenSim existing model, which has been scaled to the subject for which the experimental data were available.The main objective is to study the consistency of the model when MTGs are added to it.

For this purpose, two studies will be carried out: a torque-driven version (see Figure 15a) and a version where MTGs have been implemented (see Figure 15b). Similarly to the pendulum, the torque generators in the first model are external moments τ_i at each joint $i \in \{1, 2, ..., 7\}$; whereas in the second model a pair of muscle torque generators τ_i^{MF} and τ_i^{ME} are acting at each joint. Note that both models contain the residual forces and moment acting in the pelvis, but neither an external moment nor a pair of MTGs are applied in it such as in the rest of joints.

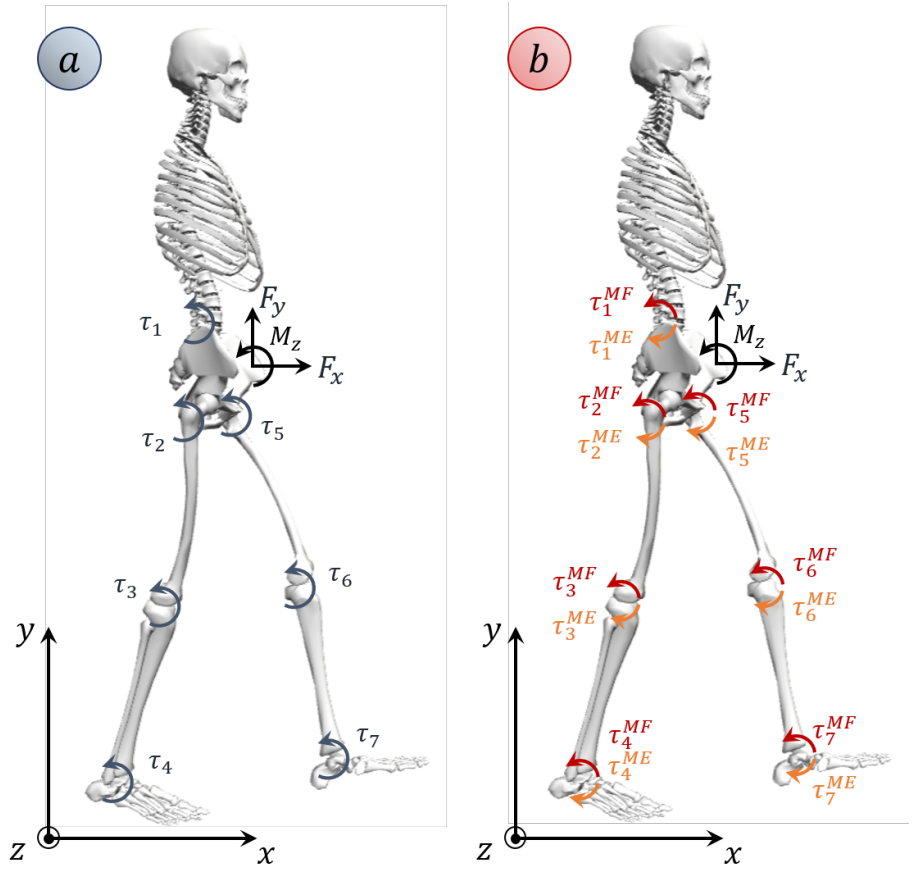

Figure 15: 2D HAT configuration as a (a) torque-driven model (b) MTGs-based model.

Finally, both models will be compared with experimentally obtained data, which include the coordinates q_{exp} as well as the torques τ_{exp} involved in the tracking. These data were obtained from markers and force plates respectively and were collected in a previous study [22]. Therefore, in this problem, an optimal control framework that tracks experimental data will be applied in both 2D HAT models.

3.2.1 MTGs modelling

In this study, the human body is modelled as a sagittal-plane multibody system that is actuated by agonist and antagonist pairs of muscle torque generators at each joint. In comparison to the simple pendulum problem, apart from studying several joints, other parameters in relation to the suppression of vibrations in the model as well as the incorporation of passive elements will be considered. Then, the net torque at each of the model's joints is the sum of the signed flexor and extensor muscle torques acting at that joint and joint damping [19]:

$$\tau_i = \tau_i^{MF} + \tau_i^{ME} - \beta \dot{q}_i \tag{5}$$

Since each muscle torque acts in a single direction, there are two MTGs acting at the joint, a flexor τ_i^{MF} and an extensor τ_i^{ME}, for a total of 14 MTGs for the whole model. The parameter β corresponds to joint damping coefficient defined at Equation 7 and $\dot{q}_i$ is the derivative of the coordinate q_i (*i.e.*, the angular velocity acting at the joint i).

The torque τ^M developed by a single MTG is given by [19]:

$$\tau^M = \tau_o^M \left(a\mathbf{f}^A(q)\,\mathbf{f}^V(\dot{q}) + \mathbf{f}^{PE}(q)\left(1 - \beta^{PE}\frac{\dot{q}}{\dot{q}_{max}^M}\right)\right) \tag{6}$$

The torque developed by equation 6 is a function of the control input a from the solver (in this case mapped to the activation of the muscle), the angle q, and angular velocity $\dot{q}$ of the joint. The angle of the joint changes the value of $\mathbf{f}^A(q)$, the passive torque-angle curve. The angular velocity of the joint affects the value of $\mathbf{f}^V(\dot{q})$, the torque velocity curve, and also the damping torque of the passive element. A non-linear normalized damping term β^{PE} is added to the passive element to suppress possible vibrations. This parameter is usually set to 0.1 in muscles and thus, it was also decided to keep that value in this model. Another parameter that is taken into account when passive elements are considered is $\dot{q}_{max}^M$, which corresponds to the maximum angular velocity achieved by the joint. Note that this value changes depending whether the torque is the flexor or the extensor. Finally, τ_o^M is the maximum isometric torque achieved by the joint. Similarly to the maximum angluar velocity, τ_o^M is also dependant on the nature of the torque and thus, it will be different for both the flexor and extensor torques.

The light damping at the joint in Equation 5 is the passive damping introduced by the musculature and tissue surrounding the joint. The damping coefficient is defined as [19]:

$$\beta = \eta\frac{\tau_o^{MF} + \tau_o^{ME}}{\dot{q}_{max}^{MF} + \dot{q}_{max}^{ME}} \tag{7}$$

Therefore, the amount of damping is proportional to the strength of the musculature and inversely proportional to its maximum angular velocity. The parameter η is a normalized joint damping scaling factor and it can take the values 0.2 or 0.4 depending on which kind of joint is studied. The first value corresponds to lower body joints and the latter to arms. Since the model used in this thesis only accounts on lower body joints, then η is set to 0.2.

Several literature sources are used to build the characteristic curves for the MTGs (see "MTG Parameters" at Table 3). Regarding the musculotendon characteristic curves, the torque-angle and torque-velocity curves have been described as in the pendulum problem (see Equation 3 and Equation 4) but transferred to several joints. While the parameters p, h and k that define the first mentioned curve change according to Table 3 (refer now to "f Parameters"), the parameters that define the torque velocity curve k_{CE1}, k_{CE2} and f_{max} are kept as in the pendulum formulation 3.1.1. Finally, the passive torque angle curve is defined according to the literature [28] as:

$$\mathbf{f}^{PE}(q) = \frac{e^{(k_{PE}\cdot q - l_0)/\varepsilon_0^M} - 1}{e^{k_{PE}} - 1} \tag{8}$$

The parameter k_{PE} is a shape factor, ε_0^M is the parallel element strain and l_0 is the slack angle which is different for each joint. These parameters are represented at Table 3 as well.

Table 3: Parameters that define the characteristic curve of the MTG in the 2D HAT problem.

MTG Parameters	Lumbar		Hip		Knee		Ankle		References
	Extension	Flexion	Extension	Flexion	Extension	Flexion	Extension	Flexion	
τ_0 (Nm)	275.1	211.7	175.7	157.3	285.6	98.60	127.6	44.30	Millard 2017 [19]
$\dot{q}_{max}$ (rad/s)	0.38	0.65	12.00	12.40	16.60	22.40	8.00	10.70	JacksonMI [16]
β_{PE}	0.1		0.1		0.1		0.1		Anderson 2007 [8]
η	0.2		0.2		0.2		0.2		Millard 2017 [19]

f Parameters		Lumbar	Hip	Knee	Ankle
f^A	h	0.210	0.720	1.042	-0.275
	k	1	1	1	1
	p	-0.173	-0.380	-0.270	-0.089
fPE	k_{PE}	3	3	3	3
	ε_0^M	0.5	0.5	0.5	0.5
	l_0	0.19	0.70	1.40	-0.10

ETSEIB

3.2.2 Optimal control tracking problem

The tracking problem formulation depends on the studied model as well. Therefore, two different optimal control statements are considered: a torque-driven formulation (see Table 4) and an MTG-driven one (see Table 5). A remarkable fact, in comparison to the predictive statement, is that experimental data q_{exp} and τ_{exp} are required to solve the problem. Note that a new path constraint $f_{residual}$ is added in the 2D HAT model. This constraint indicates that the residual forces and torque that act in the pelvis relative to the ground have to be zero in order to make the system dynamically consistent. Finally, states and controls are bounded in both formulations within minimum and maximum values, which contemplate a certain tolerance, from the experimentally obtained data.

Regarding the MTG formulation it is remarkable that a new control $\dot{a}$ is considered. It corresponds to the derivative of muscle activation and it has been taken into account as a control in order to provide a smoother evolution of muscle activations. Also note that no reserve actuator has been taken into account. This is because in an initial test it was found that the MTGs were already strong enough to perform the entire motion. Finally, it is important to mention that the MTG cost function to minimise is not totally defined as it depends on some weight factors w_i. The choice of these factors are discussed in the following section 3.2.3.

Table 4: 2D HAT Torque-driven optimal control statement.

	Torque-driven
States	q,$\dot{q}$
Controls	$\ddot{q}, \tau$
Path constraints	$f_{residual} = 0$ $\tau = \tau^{IDA}$
Cost function	$J = \sum_{i=1}^{n_q}(q_i - q_{exp_i})^2 + 0.1\sum_{i=1}^{n_q}(\tau_i - \tau_{exp_i})^2 + 0.01\sum_{i=1}^{n_q} a_i^2$

Table 5: 2D HAT MTG-driven optimal control statement.

	MTG-driven
States	q,$\dot{q}, a$
Controls	$\ddot{q}, \tau, \dot{a}$
Path constraints	$f_{residual} = 0$ $\tau = \tau^{IDA}$ $\tau_i = \tau_i^{MF} + \tau_i^{EF}$
Cost function	$J = w_1\sum_{i=1}^{n_q}(q_i - q_{exp_i})^2 + w_2\sum_{i=1}^{n_q}(\tau_i - \tau_{exp_i})^2 + w_3\sum_{i=1}^{n_q}\dot{a}_i^2 + w_4\sum_{i=1}^{n_q}\ddot{q}_i^2$

Similary to the simple pendulum, in order to implement the optimal control algorithm, we used $GPOPS-II$, which works within a $MATLAB$ environment.

3.2.3 Simulations of interest

The main objective of this study is to obtain a model that includes muscle torque generators in which both the coordinates and the moments involved are as close as possible to reality. Therefore, several studies will be carried in order to obtain the MTG model configuration that provides best results in terms of tracking the experimental data. An important fact to take into account is that all the simulations in the 2D HAT model only account on the 80% of the gait cycle. That is due to the fact that the there are only measurements for a double support, as in the other, one foot is outside the plates. The final configuration of the MTG model will be compared to the torque-driven version.

The first study consists in changing the weights from the cost function in the MTG formulation (see Table 6). Hence, the cost function that leads to better results will be taken into account in the following study. Note that from each cost function proposed, only one weight factor is changed with respect to the first one.

Table 6: Set of cost functions studied.

Cost function	w_1	w_2	w_3	w_4
A	1	0.1	0.001	0.01
B	1	1	0.001	0.01
C	1	0.1	0.01	0.01
D	1	0.1	0.001	0.1

Once the best cost function has been chosen, a second study will be conducted looking at the relevance of the joint damping parameters and passive elements. The configuration that shows better results in terms of tracking the experimental data, will finally be compared with the torque-driven model. Figure 16 shows a diagram which represents the process that is carried out in order to obtain the final version of the MTG model.

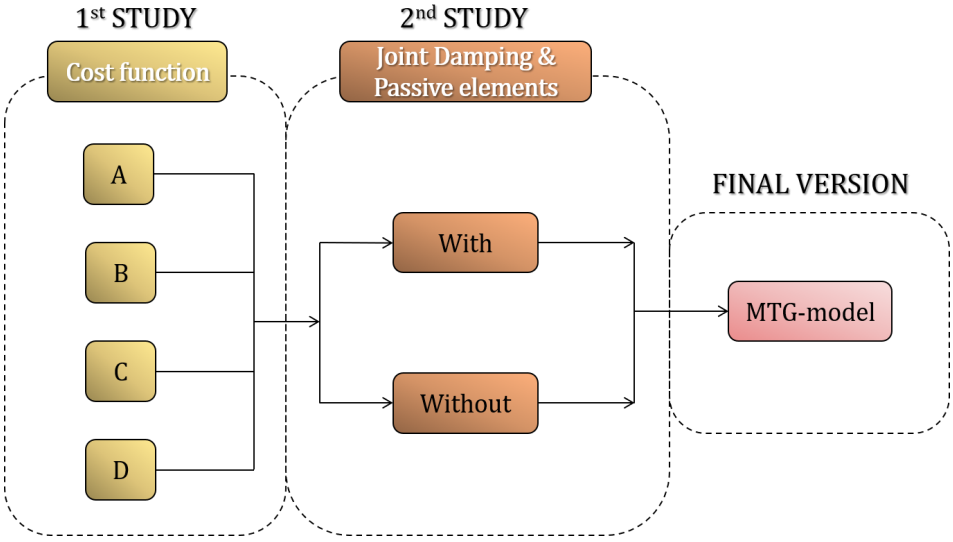

Figure 16: Process that leads to the final version of the MTG model.

The final study will take into account which of the two models shows more similarities with respect to the experimentally obtained data, as well as the time and number of iterations required for each version to achieve the optimal solution. In order to quantify how well the tracking is performed, the Root Mean Square Error (RMSE) (see Equation 9) is considered.

$$RMSE(x_i) = \sqrt{\frac{1}{K}\sum_{j=1}^{K}(x_{i,j} - x_{exp_{i,j}})^2} \tag{9}$$

The parameter K is the total number of frames of the gait cycle; $x_{i,j}$ is the i^{th} component of the optimal control problem $x \in \{q, \tau\}$ at the j^{th} frame; and $x_{exp_{i,j}}$ the i^{th} component reference vector obtained from the experimental capture $x_{exp} \in \{q_{exp}, \tau_{exp}\}$ at the j^{th} frame.

4 Results and discussion

The purpose of this section is to show and discuss the results obtained by applying the methodology explained in section 3. Similarly to that section, this section will be divided in two: a first part focusing on the pendulum problem and a second part focusing on the human gait problem.

4.1 Simple pendulum predictive problem

In this problem, several simulations are carried out based on different intitial and final conditions (see Figure 13). The purpose of this section is to discuss the dynamics behind the predictive problem, *i.e.*, how the different states evolve in order to minimise the cost function while satisfying the constraints at the same time when different conditions and models are considered.

4.1.1 Simulation I

The first situation to be studied consists of varying the pendulum coordinate from an initial state $q_{ini} = -70^o$ to a final value of $q_{fin} = -20^o$ (see Figure 17).

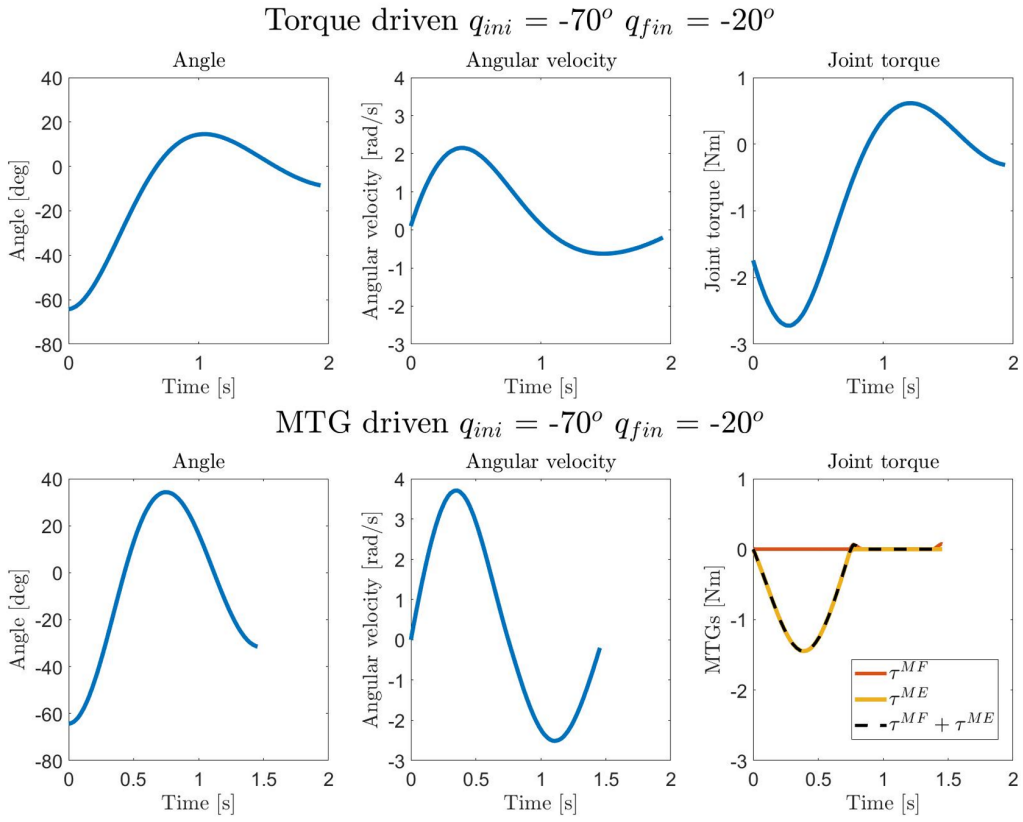

Figure 17: Evolution of states and joint torque in the torque-driven model and the MTG-driven model when Simulation I is conducted.

As can be seen in both models, the pendulum goes through positive angles instead of going directly to the desired position. Otherwise, the pendulum would have to stop very suddenly, which would imply a very high deceleration. This would lead to the application of an external negative momentum (in the opposite sense to the natural evolution of the state due to gravity) of a very high value. Therefore, the cost function would be more difficult to minimise. It is for this reason that the optimal motion goes through such positive angles.

Another remarkable fact is that in the torque-driven model there is always some external moment applied, whereas in the MTG only the extensor torque is considered. More specifically, when the pendulum reaches its maximum angle it also changes the joint torque monotony. While in the MTG version only a very few from the flexor torque is required to go back to the desired position, in the torque-driven model a bit more torque is needed.

4.1.2 Simulation II

In the second situation studied the initial and final positions are changed in respect to the previous study and thus, the pendulum changes from an inital postion $q_{ini} = -20^o$ to a final position $q_{fin} = -70^o$ (see Figure 18).

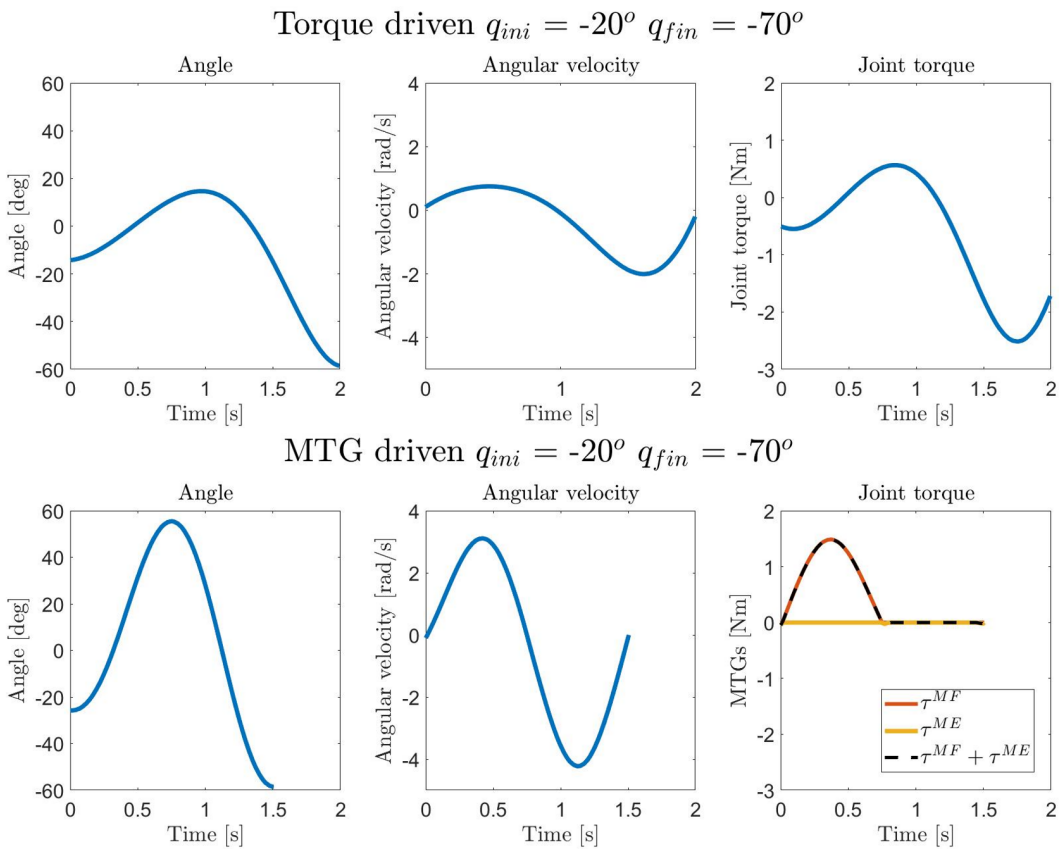

Figure 18: Evolution of states and joint torque in the torque-driven model and the MTG-driven model when Simulation II is conducted.

Similarly to the first study, the pendulum goes through positive angles as well, instead of going directly to the desired position. However, in comparison to the first study, the torque needed to conduct this motion has opposite sense. Hence, only the flexor torque is considered in the MTG version. That is due to the fact that initial and final conditions have been changed from the previous simulation. Note again that once the maximum position is reached, no torques are involved in the MTG model. Nonetheless, the torque-driven version presents its highest value there since it needs to slow down when the pendulum is reaching its final position.

4.1.3 Simulation III

In comparison to the rest of studies, the third situation is the one that encompasses more range of motion, thus varying from an initial angle $q_{ini} = -70^o$ to a final one $q_{fin} = 70^o$ (see Figure 19). Also note that given the symmetry of the problem, both states (q and $\dot{q}$) as well and the joint torque evolve as symmetric functions.

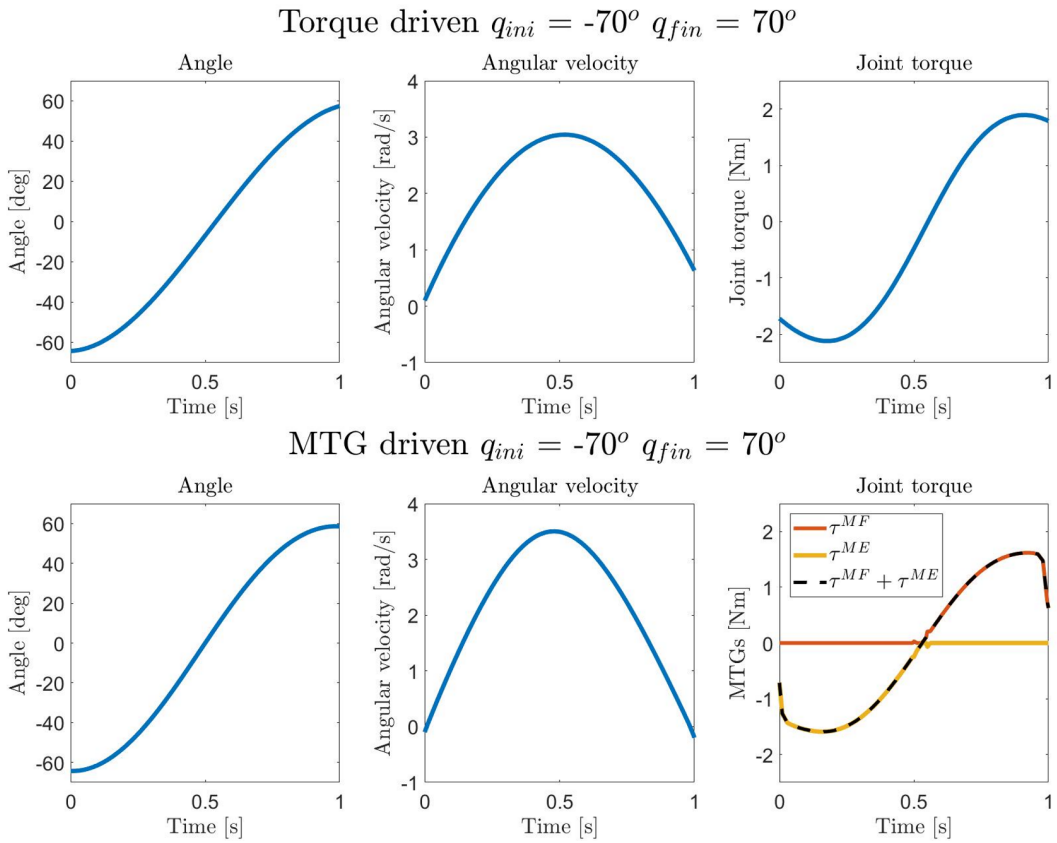

Figure 19: Evolution of states and joint torque in the torque-driven model and the MTG-driven model when Simulation III is conducted.

Now, if both models are compared, there is almost no difference between the torque-driven version and the MTG one. Regarding the joint torque in the MTG model, an extensor torque is applied at the beginning of the motion as it tries to diminish the initial acceleration. Conversely, when the pendulum is reaching the final configuration, a flexor torque will be employed in order to reduce the value of the deceleration. A similar situation occurs in the case of the torque-driven, although with a single torque.

4.1.4 Simulation IV

The last situation studied changes the the angle from an initial value of $q_{ini} = -20^o$ to a final value that is $q_{fin} = 70^o$ (see Figure 20).

As it happened in the third study, the pendulum reaches its final position without the need of moving back and forth as it happened in the first two cases. One more time, the predicted motion in both models is quite similar between them.

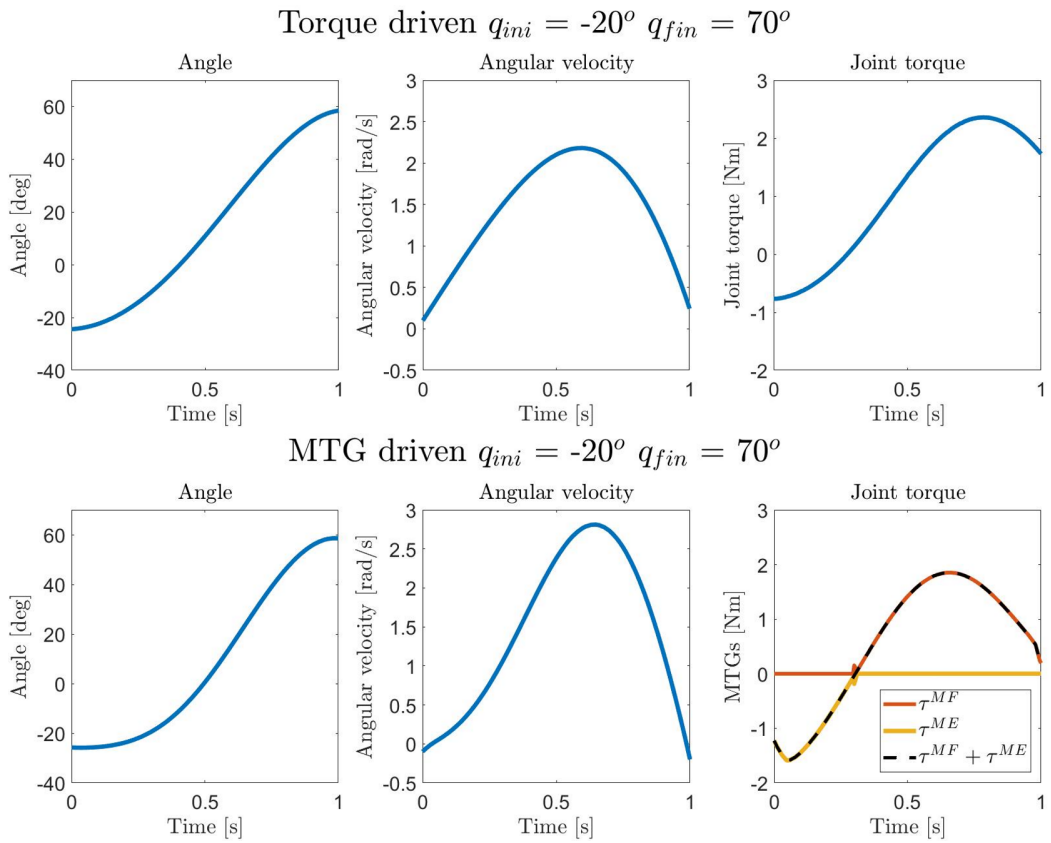

Figure 20: Evolution of states and joint torque in the torque-driven model and the MTG-driven model when Simulation IV is conducted.

It is remarkable that in comparison to the third study, the contribution of the extensor torque to the predicted motion is considerably lower than the flexor. Note that something similar happens to the torque-driven model. The main cause of this is the value of the initial angle. The higher the value, the higher the initial potential energy and hence, a higher external moment opposed to the motion would be required to slow it down to eventually reach the final position in stable conditions (*i.e.*, $\dot{q} \approx 0$).

4.1.5 General discussion

Everyhting considered, it seems that for lower ranges of motion (*i.e.*, the first two simulations) muscle torque generators models provide better results in terms of minimising the cost function. That can be clearly seen since the time to reach the optimal predicted motion is reduced compared to their respective torque-driven versions. Note in these cases that not only are the angular velocities higher, but also the joint torque is reduced and hence, the predicted results are closer to the optimal. Despite the fact that the other two simulations do not show this behaviour and thus, the difference between models is not that significant, it is still remarkable that less time is required to perform the predicted motion. Since all the simulations are equally modelled, the only reason that provokes these differences is the set of initial and final conditions. Therefore, the more natural these conditions are to the dynamics of the pendulum, the less time would be needed to perform the predicted results.

4.2 2D HAT tracking problem

The main purpose of this section is to faithfully reproduce a gait cycle by using a 2D HAT model when muscle torque generators are added to it. The more similar the coordinates and the torques are to experimentally obtained data, the better the tracking and therefore, the more reliable the model. In order to quantify how well the tracking is performed, the Root Mean Square Error (RMSE) (see Equation 9) has been taken into account throughout this section.

As it is stated in section 3.2.3, several studies are carried out in order to determine the final MTG version that will eventually be compared to the torque-driven model. Therefore, in this section it is discussed the process that leads to this final version as well as the comparison between the two models.

4.2.1 Study of different formulations in the MTG cost function

In a first attempt to choose the cost function that yields to best results in terms of tracking, we calculated the $RMSE$ of coordinates (see Table 7) and torques (see Table 8) at each joint for the different cost functions A, B, C and D previously defined in section 3.2.3. Also note that the $RMSE$ mean for each cost function is computed in both cases.

Table 7: RMSE of coordinates obtained from the different formulations.

Cost function	**Lumbar extension** [°]	**Hip flexion** [°]		**Knee angle** [°]		**Ankle angle** [°]		**Mean** [°]
		Right	Left	Right	Left	Right	Left	
A	0.81	2.66	1.83	1.86	0.91	3.16	8.84	2.87
B	1.12	3.39	2.82	2.60	1.98	3.23	6.43	3.08
C	0.73	2.82	1.74	2.02	1.12	3.23	6.58	2.60
D	0.79	3.43	2.11	3.09	2.69	3.66	6.76	3.22

Table 8: RMSE of torques obtained from the different formulations.

Cost function	**Lumbar extension** $[Nm]$	**Hip flexion** $[Nm]$		**Knee angle** $[Nm]$		**Ankle angle** $[Nm]$		**Mean** $[Nm]$
		Right	Left	Right	Left	Right	Left	
A	8.97	10.41	8.84	4.77	5.17	2.17	3.04	6.20
B	5.84	7.22	6.33	3.89	3.70	2.10	3.02	4.59
C	8.53	10.62	9.74	4.80	5.44	2.16	3.33	6.37
D	7.61	10.33	9.76	5.37	5.70	1.55	3.23	6.22

Clearly, the cost function that provides best results is B as it shows significantly lower $RMSE$ values, specially when tracking torques. The root cause of this value is that cost function B is precisely the one that has a highest weighted factor in the term where torques are involved. That leads to a higher penalization if the difference between the computed torque and the experimental one is higher as well. Bearing in mind that the differences when tracking coordinates are not that significant between the different cost functions, it was decided to keep B (see Equation 10) as the cost function in the next study.

$$J = \sum_{i=1}^{n_q}(q_i - q_{exp_i})^2 + \sum_{i=1}^{n_q}(\tau_i - \tau_{exp_i})^2 + 0.001\sum_{i=1}^{n_q}\dot{a}_i^2 + 0.01\sum_{i=1}^{n_q}\ddot{q}_i^2 \tag{10}$$

4.2.2 Influence of passive elements and joint damping in motion tracking

Similarly to the previous study, we compute the $RMSE$ to see whether adding passive elements and the joint damping to the model can indeed lead to more realistic results (see Table 9 and Table 10). Remember that these elements are added to supress possible vibrations in the musculature and thus are supposed to give a better insight into the human walking behaviour.

Table 9: RMSE of coordinates with and without passive elements (PE) and joint damping (DAMP).

DAMP & PE	**Lumbar extension** [°]	**Hip flexion** [°]		**Knee angle** [°]		**Ankle angle** [°]		**Mean** [°]
		Right	Left	Right	Left	Right	Left	
With	1.79	1.87	3.12	2.06	6.92	2.99	5.20	3.42
Without	1.12	3.39	2.82	2.60	1.98	3.23	6.43	3.08

Table 10: RMSE of torques with and without passive elements (PE) and joint damping (DAMP).

DAMP & PE	**Lumbar extension** $[Nm]$	**Hip flexion** $[Nm]$		**Knee angle** $[Nm]$		**Ankle angle** $[Nm]$		**Mean** $[Nm]$
		Right	Left	Right	Left	Right	Left	
With	7.27	6.98	7.21	3.21	3.72	1.98	2.93	4.76
Without	5.84	7.22	6.33	3.89	3.70	2.10	3.02	4.59

In this case, the final choice is not that clear. While more than half of the joints present lower $RMSE$ values when these elements are added in both cases (coordinates and torques), it is still not enough to the overall contribution. That is due to the fact that in some cases, the $RMSE$ calculated are notably higher compared to the version without these elements. Some examples are the left knee angle in coordinates or the lumbar extension in torques. If a further exploration of the parameters defining these elements was conducted, that would probably yield lower errors and hence, a better tracking.

Despite the fact that a formulation without these elements seems to provide better results, a comparison between both computational times was conducted in order to secure a final choice. The results were that the computational time with the passive elements and joint damping was more than twice as long as without them. Therefore, the final study was carried out without these elements.

4.2.3 Evaluation of muscle torque generators implementation

Once the final version of the MTG model is clearly defined, we can now proceed to the final study. As it was previously stated, in this last section, the MTG model is compared to the torque-driven model, which is a previous version of the 2D HAT model at skeletal level. Likewise the previous studies, the $RMSE$ of coordinates (see Table 11) and torques (see Table 12) at each joint will also be of interest in this final study.

Table 11: RMSE of coordinates in the torque-driven model (TD) and the MTG model.

Model	**Lumbar extension** [°]	**Hip flexion** [°]		**Knee angle** [°]		**Ankle angle** [°]		**Mean** [°]
		Right	Left	Right	Left	Right	Left	
TD	0.41	0.47	0.46	0.64	0.61	0.84	0.70	0.59
MTG	1.12	3.39	2.82	2.60	1.98	3.23	6.43	3.08

Table 12: RMSE of torques in the torque-driven model (TD) and the MTG model.

Model	**Lumbar extension** $[Nm]$	**Hip flexion** $[Nm]$		**Knee angle** $[Nm]$		**Ankle angle** $[Nm]$		
		Right	Left	Right	Left	Right	Left	**Mean** $[Nm]$
TD	3.95	4.54	6.15	2.49	2.16	1.79	1.94	3.29
MTG	5.84	7.22	6.33	3.89	3.70	2.10	3.02	4.59

When computing the $RMSE$ in the final study, we obtain considerably low values in both models, which means that the tracking is well performed in both cases. More specifically, if we take a look at the obtained errors in torques, we note that in general the difference between models is quite low. For instance, the obtained $RMSE$ for the left hip flexion torque in the torque-driven model is $6.15\ Nm$ and similarly, a value of $6.33\ Nm$ in the MTG version is obtained. Nonetheless, in some joints the difference between models is still relevant. For instance, the joint in the MTG model that presents the maximum relative error obtained when tracking coordinates is the left ankle with an $RMSE$ value of 6.43^o compared to 0.70^o in the torque-driven version.

Since the $RMSE$ only takes into account the average error between functions, it is decided to complement this information with an evolution of the coordinates and torques for each joint. If we take a look at Figure 21 a more detailed comparison between the tracking motion in both models is carried out. Therefore, it is possible to check if the tracked results show a similar tendency to the experimental data. In order to ease the visualization of the results, only left joints were plotted. We decided to show left joints instead of the right ones because the stance phase begins with the left leg.

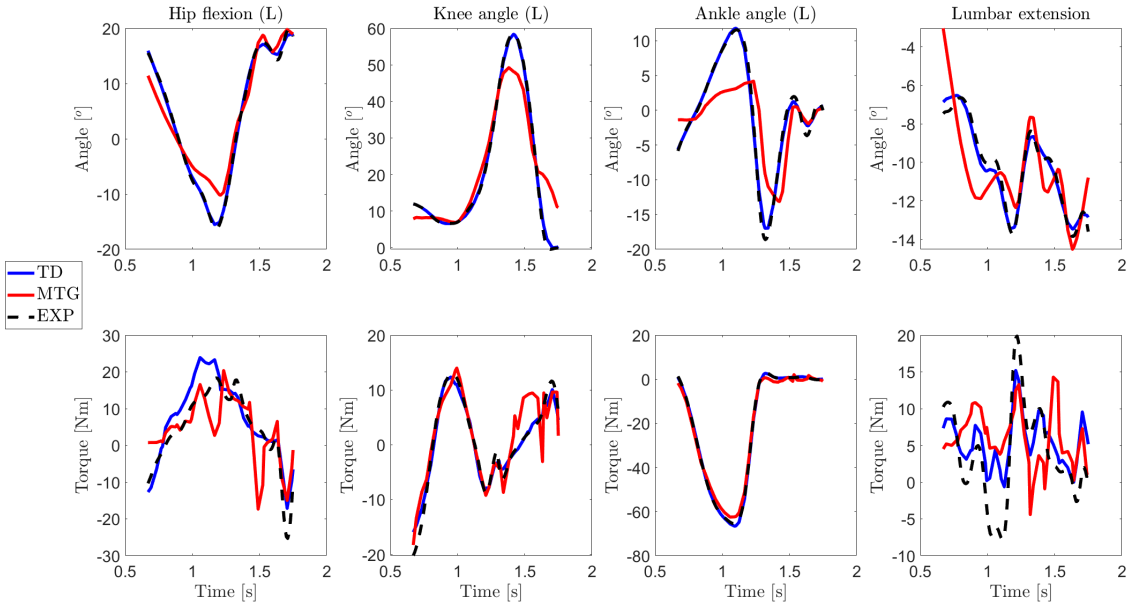

Figure 21: Tracking of coordinates and torques in a 2D HAT model based in a torque-driven (in blue) and an MTG (in red) versions. Experimental data is shown with a dashed black line. The gait accounts the 80% of the cycle and left joints are shown.

If we take a look at the hip left flexion again, it is possible to see that despite the fact that $RMSE$ in torques is similar between models, the error is still a bit high compared, for example, to the tracked torque in the ankle angle. The hip flexion angle shows much better results than its torque version. Note that when MTGs are considered in coordinates, a slight difference in the peak value is produced. Nontheless, the rest of the tracking is generally adequate.

Moving now to the knee angle, similar results to the hip flexion are obtained. For instance, there is also a small difference between the peak values in the tracked coordinates when MTGs are employed, but the rest of the tracking is fine. If we now analyse the torques, the torque-driven model seems that is performing a better tracking. That can also be explained through the $RMSE$ obtained. While the value obtained with the torque-driven version is only $2.16\ Nm$, when we apply MTGs a value of $3.70\ Nm$ is reported.

As it was previously stated, the ankle angle shows the maximum relative error in terms of coordinate tracking when MTGs are applied. However, the tendency of it is still adequate. Moving now to the torque tracking analysis, we observe an almost perfect tracking in both models. This notorious difference between coordinates and torques suggests that further exploration regarding the MTG implementation in the ankle should be undertaken.

Finally, if we give some insight into the observed results in the lumbar extension angle, the torque-driven model provides better results again, especially at the beginning of the motion. Nonetheless, the tendency of the tracking is correct and generally well adjusted to the experimentally obtained data. Conversely, tracking in torques are a bit further from the experimental values. Similarly to the hip flexion case, both models perform a similar tracking while none of them is perfectly adjusted to the experimental data.

In order to give a deeper insight into the pairs of muscle torque generators involved in each joint, we decided to break them down into their flexor and extensor part. Figure 22 shows the contribution of each MTG pair throughout the cycle.

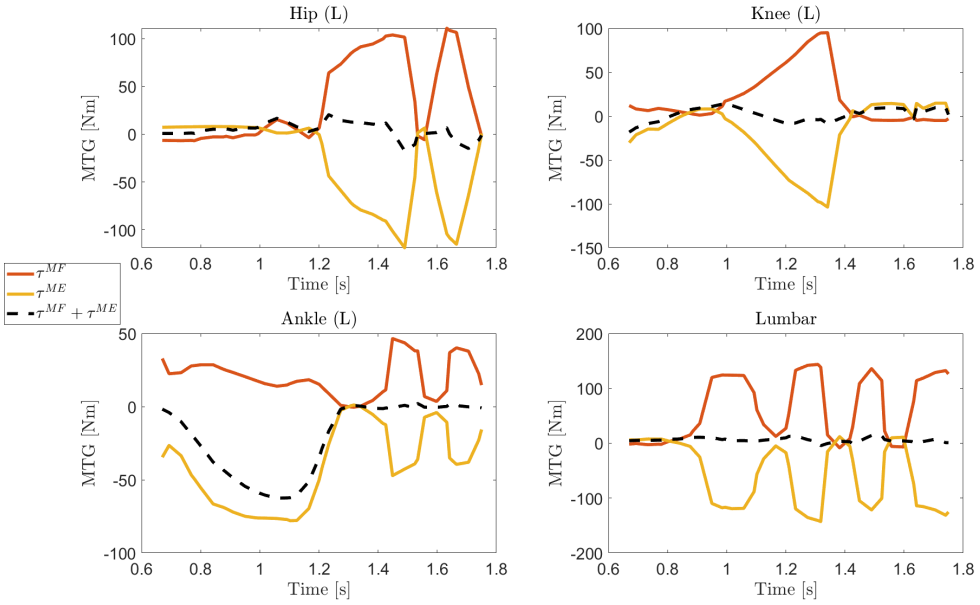

Figure 22: Pairs of muscle torque generators at each left joint and lumbar.

Two remarkable facts can be seen clearly seen in Figure 22. On the one hand, the different MTG pairs are almost symmetric to one another, except in the left ankle at the beginning of the gait cycle, in which a higher contribution of the extensor torque is reported. On the other hand, we obtained quite high unexpected values in some parts of the cycle in each of the joints. Bearing in mind how these pairs of MTGs are calculated in the final version of the MTG model (see Equation 11), all terms are the same except the isometric maximum torque τ_o and the muscle activations a.

$$\tau_i^M = \tau_o^M a \mathbf{f}^A(q)\, \mathbf{f}^V(\dot{q}) \tag{11}$$

Therefore, a further exploration in these two parameters could be conducted in order to gain better insight into the contribution of each the flexor and extensor torques in the gait cycle.

4.2.4 General discussion

By and large, the tracking performed when muscle torque generators are taken into account is adequate since no extreme $RMSE$ are reported nor any undesired tendency in the tracking is observed for the plotted joints. It is also remarkable that a better tracking in the torques is achieved in comparison to the coordinates. However, the tracking is still better performed by the torque-driven model, especially when tracking coordinates. That is probably due to the fact that the cost function considered in the MTG-driven model penalizes more the torque errors rather than the coordinate ones. Therefore, if we wanted to obtain better results in terms of tracking coordinates new readjustments in the cost function should be considered.

Another fact that has not yet been mentioned in this section is the computational time as well as the iterations needed to obtain the optimal solution. Table 13 shows both the time and the number of iterations that the solver needed to converge to an optimal solution in the studied tracking problem.

Table 13: Computational time and number of iterations required in both models

	Time [s]	**Iterations**
TD	2.91	23
MTG	92.87	1403

As it was expected, the model in which muscle torques generators are employed shows higher values in both the computational time and number of iterations. That is because more restrictions have to be satisfied in the optimal control formulation regarding the torques in comparison to the torque-driven version.

Finally, despite the fact that the tracking performed by the MTG model is correct, it was expected that the model had provided a more realistic behaviour in comparison to the torque-driven model. That is due to the fact that still further explorations need to be conducted in some of the parameters that define the pairs of MTGs before this model is employed for other purposes such human motion prediction. Parameters such as the maximum isometric torque or the characteristic musculotendon curves involved in each pair of the MTGs could be more in depth investigated to gain better insights.

5 Project impact

In this section we provide a detailed explanation about the economic cost of the project. Besides, we contemplate the environmental impact produced in this work. .

5.1 Economic cost

The economic cost of the project is based on four different aspects: the depreciation of the computer used for the simulations, the *MATLAB* and *GPOPS-II* licenses, the working time (student and supervisors), and finally, the electrical energy consumed.

Depreciation is calculated from the total price of the electronic device, its useful time and the total time it has been used. The useful life of the computer is considered to be 4 years, which corresponds to a total of 35040 hours. Finally, the laptop has been used for an amount of 320 hours during the thesis.

MATLAB and *GPOPS-II* licenses expire after one year. Therefore, their useful life is about 8760 hours. Considering that the software was used only during half of the hours when the computer was used, it is then estimated that both *MATLAB* and *GPOPS-II* have been used for a total of 160 hours.

Regarding the student's hours of dedication, it should be taken into account the time in which the computer was used (320 hours), plus 30 hours of meetings, calculations and reflections. The hours of support and supervision are considered to be 40 hours in total (considering both supervisors).

Finally, the electrical power of light and computers have been estimated to be 35 W for each of them. A light bulb was only switched on during the hours of less light (a total of 100 hours) and the computer during the previously mentioned 320 hours. We assumed constant the price of electricity, with a value of 0.29 €/kWh.

As can be seen in Table 14, the total cost of the project is 3428.28 €.

Table 14: Calculation of the final project cost. Variable costs of the computer and licenses are obtained from dividing their fixed cost by their useful life in hours. Variable cost of electrical energy is found from its price multiplied by the power consumption of computers and light.

	Fixed cost [€]	**Useful life [years]**	**Variable cost [€/h]**	**Time spent in the project [h]**	**Cost related to the ptoject [€]**
Laptop	750	4	0.0214	320	6.85
MATLAB license	840	1	0.0959	160	15.34
GPOPS-II license	100	1	0.0114	160	1.83
Student	-	-	8	350	2800.00
Supervisors	-	-	15	40	600.00
Electrical energy	-	-	0.0102	420	4.26
TOTAL COST					**3428.28 €**

5.2 Environmental impact

The environmental impact of this project is minimal since the main studies were based on simulations using a computer at home. However, electricity and electronic devices such as a laptop and a tablet can be considered.

Regarding the electrical consumption, a computer and a light bulb have been assumed to be switched on while working on the thesis. However, their consumption is marginal and thus, they are not considered to have such a negative environmental impact in the project.

When evaluating the deterioration of the electronic devices we have to take into account that once their useful life is finished, they must be treated individually. This evaluation is in agreement with the Regulation 2017/699 [34], which establishes a common methodology for the calculation of the weight of electrical and electronic equipment (EEE) as well as for the calculation of the quantity of waste in electrical and electronic equipment (WEE).

Conclusions

In this bachelor's thesis, optimal control techniques have been applied to both the prediction of a new motion and the tracking of a known one. In order to implement the optimal control algorithm, we used $GPOPS-II$, which works in $MATLAB$. Therefore, there has been a process of getting acquainted with optimal control theory and its environment.

In both formulations, a torque-driven model (*i.e.*, at skeletal level) is obtained from the $OpenSim$ repository. Subsequently, we employed muscle torque generators with $MATLAB$ in each of them as an alternative of detailed musculoskeletal models.

Regarding the predictive problem when using a simple pendulum model, muscle torque generators were slightly advantageous than its torque-driven version when the studied simulation encompassed a shorter range of motion. Conversely, when using a 2D HAT model for human gait tracking, despite the fact that the tracking performed with MTGs was adequate, a more realistic behaviour than its torque-driven version was expected.

This project can be considered a first research work in muscle torque generators modelling in the Biomechanical Engineering Lab (BIOMEC) at UPC. Thus, further studies would need to be conducted in order to obtain more realistic models. Parameters such as the maximum isometric torque or the characteristic musculotendon curves involved in each pair of the MTGs could be more in depth investigated to gain better insights.

Acknowledgements

I would like to express my sincere thanks to my supervisors, Míriam Febrer Nafría and Josep María Font Llagunes, for their support, advice and for giving me the opportunity to work for the first time in a research group such as the BIOMEC Lab. I want to give thanks especially to you, Míriam, for the weekly meetings, for your constant feedback until the end of the project, and for being able to highlight the well done work as well.

Moreover, I would like to thank family and friends for supporting me when things did not come that easily and for always showing interest in each of the small (or big) advances in the project.

References

[1] Marko Ackermann and Werner Schiehlen. "Dynamic Analysis of Human Gait Disorder and Metabolical Cost Estimation". In: *Archive of Applied Mechanics* 75 (Sept. 2006), pp. 569–594. DOI: 10.1007/s00419-006-0027-7.

[2] A. Alamdari and V.N. Krovi. "Chapter Two - A Review of Computational Musculoskeletal Analysis of Human Lower Extremities". In: *Human Modelling for Bio-Inspired Robotics*. Ed. by Jun Ueda and Yuichi Kurita. Academic Press, 2017, pp. 37–73. ISBN: 978-0-12-803137-7. DOI: https://doi.org/10.1016/B978-0-12-803137-7.00003-3. URL: https://www.sciencedirect.com/science/article/pii/B9780128031377000033.

[3] BBC. *Muscular system. Agonist and antagonist muscle pairs.* URL: https://www.bbc.co.uk/bitesize/guides/z8stfrd/revision/4. (accessed: 15.06.2022).

[4] Peter Brown and John McPhee. "A 3D ellipsoidal volumetric foot–ground contact model for forward dynamics". In: *Multibody System Dynamics* 42 (Apr. 2018). DOI: 10.1007/s11044-017-9605-4.

[5] Jeremy C O'Connor Christopher L Vaughan Brian L Davis. *Dynamics of Human Gait*. Kiboho Publishers, 1992. ISBN: 0-620-23558-6.

[6] David Civantos. "Study of the foot-ground contact model for the prediction of human gait". In: (July 2020). DOI: https://upcommons.upc.edu/handle/2117/349395.

[7] Matthew Millard Thomas Uchida Ajay Seth Scott L. Delp. "Flexing Computational Muscle: Modeling and Simulation of Musculotendon Dynamics". In: *Journal of Biomechanical Engineering* 135 (Feb. 2013), pp. 70–77. DOI: https://doi.org/10.1115/1.4023390.

[8] Michael L. Madigan Dennis E. Anderson and Maury A. Nussbaum. "Maximum voluntary joint torque as a function of joint angle and angular velocity: Model development and application to the lower limb". In: *Journal of Biomechanics* 40 (Mar. 2007), pp. 3105–3113. URL: https://www.sciencedirect.com/journal/journal-of-biomechanics.

[9] OpenSim Documentation. *Characteristic Musculotendon Curves*. URL: https://simtk-confluence.stanford.edu:8443/display/OpenSim/Characteristic+Musculotendon+Curves. (accessed: 31.05.2022).

[10] Marcus G. Pandy Frank C. Anderson. "Dynamic Optimization of Human Walking". In: *Journal of Biomechanical Engineering* 123 (Oct. 2001), pp. 381–390. DOI: 10.1115/1.1392310. URL: chrome-extension://efaidnbmnnnibpcajpcglclefindmkaj/https://homes.cs.washington.edu/~todorov/courses/amath533/AndersonPandy.pdf.

[11] Benjamin Fregly. "Design of Optimal Treatments for Neuromusculoskeletal Disorders using Patient-Specific Multibody Dynamic Models". In: *International journal for computational vision and biomechnanics* 2 (July 2009), pp. 145–155.

[12] Benjamin J. Fregly. "A Conceptual Blueprint for Making Neuromusculoskeletal Models Clinically Useful". In: *Applied Sciences* 11.5 (2021). ISSN: 2076-3417. DOI: 10.3390/app11052037. URL: https://www.mdpi.com/2076-3417/11/5/2037.

[13] Friedl De Groote - Allison L Kinney - Anil V Rao - Benjamin J Fregly. "Evaluation of Direct Collocation Optimal Control Problem Formulations for Solving the Muscle Redundancy Problem". In: *Epub* 44(10) (Oct. 2016), pp. 2922–2936. DOI: 10.1007/s10439-016-1591-9.

[14] Archibald Vivian Hill. "The heat of shortening and the dynamic constants of muscle". In: *Proc. R. Soc. Lond.* 126 (Oct. 1938). DOI: B126136âĂŞ195.

[15] McNally W Inkol K.A. Brown C. "Muscle torque generators in multibody dynamic simulations of optimal sports performance". In: *Multibody System Dynamics* 50 (Dec. 2020), pp. 435–452. DOI: 10.1007/s11044-020-09747-9. URL: https://link.springer.com/article/10.1007/s11044-020-09747-9.

[16] Monique Iris Jackson. "The mechanics of the table contact phase of gymnastics vaulting". PhD thesis. Loughborough University, 2010.
[17] Oliver Jones. *Anatomical Planes*. URL: https://teachmeanatomy.info/the-basics/anatomical-terminology/planes/. (accessed: 26.05.2022).
[18] Matthew Millard and Katja Mombaur. "A Quick Turn of Foot: Rigid Foot-Ground Contact Models for Human Motion Prediction". In: *Frontiers in Neurorobotics* 13 (2019). ISSN: 1662-5218. DOI: 10.3389/fnbot.2019.00062. URL: https://www.frontiersin.org/article/10.3389/fnbot.2019.00062.
[19] Matthew Millard, Manish Sreenivasa, and Katja Mombaur. "Predicting the Motions and Forces of Wearable Robotic Systems Using Optimal Control". In: *Frontiers in Robotics and AI* 4 (2017). ISSN: 2296-9144. DOI: 10.3389/frobt.2017.00041. URL: https://www.frontiersin.org/article/10.3389/frobt.2017.00041.
[20] Rosa Pàmies-Vilà Míriam Febrer-Nafría and Josep M. Font-Llagunes. "Foot-ground contact modelling for computational prediction of human walking motion". In: *The 5th Joint International Conference on Multibody System Dynamics* (June 2018). DOI: https://upcommons.upc.edu/handle/2117/122816.
[21] Míriam Febrer Nafría. *Application of optimal control in the simulation of human motion*. 2016.
[22] Míriam Febrer Nafría. "Optimal control prediction of assisted walking using torque-driven models. Application to active orthosis simulation to assist individuals with spinal cord injury". PhD thesis. Universitat Politècnica de Catalunya, 2020.
[23] Valerie Theresa Norman-Gerum. "Predictive Dynamic Simulation of Healthy Sit-to-Stand Movement". PhD thesis. University of Waterloo, 2019.
[24] Roger Pallarès. "Optimal Control Prediction of Dynamically Consistent Walking Motions". In: (June 2017). DOI: https://upcommons.upc.edu/handle/2117/111033?show=full.
[25] Rosa Pàmies-Vilà et al. "Use of performance indicators in the analysis of running gait impacts". In: *Multibody System Dynamics* 43 (June 2018). DOI: 10.1007/s11044-017-9580-9.
[26] Walter Pirker and Regina Katzenschlager. "Gait disorders in adults and the elderly: A clinical guide". In: *Wiener klinische Wochenschrift* 129 (Oct. 2016). DOI: 10.1007/s00508-016-1096-4.
[27] Dan Robbins. "Chapter 7 - Muscle biomechanics". In: *Human Orthopaedic Biomechanics*. Ed. by Bernardo Innocenti and Fabio Galbusera. Academic Press, 2022, pp. 121–135. ISBN: 978-0-12-824481-4. DOI: https://doi.org/10.1016/B978-0-12-824481-4.00009-3. URL: https://www.sciencedirect.com/science/article/pii/B9780128244814000093.
[28] F. Romero and F. J. Alonso. "A comparison among different Hill-type contraction dynamics formulations for muscle force estimation". In: *Mechanical Sciences* 7.1 (2016), pp. 19–29. DOI: 10.5194/ms-7-19-2016. URL: https://ms.copernicus.org/articles/7/19/2016/.
[29] G. Serrancoli, J. De Schutter, and F. De Groote. "Analysis of optimal control problem formulations in skeletal movement predictions". In: *International Conference on NeuroRehabilitation*. Springer, Oct. 2016. URL: http://hdl.handle.net/2117/102179.
[30] M. P. Silva and J. A. C. Ambrósio. "Kinematic data consistency in the inverse dynamic analysis of biomechanical systems. Multibody System Dynamics". In: *Multibody System Dynamics* 8.2 (2001), pp. 219–239. DOI: https://www.academia.edu/17930205/Kinematic_data_consistency_in_the_inverse_dynamic_analysis_of_biomechanical_systems.
[31] Manish Sreenivasa et al. "Optimal Control Based Stiffness Identification of an Ankle-Foot Orthosis Using a Predictive Walking Model". In: *Frontiers in Computational Neuroscience* 11 (2017). ISSN: 1662-5188. DOI: 10.3389/fncom.2017.00023. URL: https://www.frontiersin.org/article/10.3389/fncom.2017.00023.

[32] Maximilian Stelzer and Oskar von Stryk. "Efficient Forward Dynamics Simulation and Optimization of Locomotion: From Legged Robots to Biomechanical Systems". In: *Proc. 3rd Intl. Symposium on Adaptive Motion in Animals and Machines* (*AMAM*) 129 (Sept. 2005).

[33] Darryl G Thelen. "Adjustment of muscle mechanics model parameters to simulate dynamic contractions in older adults". In: *Journal of Biomechanical Engineering* 125 (Feb. 2003), pp. 70–77. DOI: 10.1115/1.1531112.

[34] European Union. "Commission Implementing Regulation (EU) 2017/699". In: *Official Journal of the European Union* (Apr. 2017). DOI: chrome-extension://efaidnbmnnnibpcajpcglclefindmka https://eur-lex.europa.eu/legal-content/EN/TXT/PDF/?uri=CELEX:32017R0699&from=EN.

[35] David A. Winter. *The Biomechanics and motor control of human gait*. 1987. ISBN: 0-88898-078-7.

[36] Gary T. Yamaguchi. *Dynamic Modeling of Musculoskeletal Motion: A Vectorized Approach for Biomechanical Analysis in Three Dimensions*. 2001.

[37] Junyan Li Zhongmin Jin and Zhenxian Chen. *Computational Modelling of Biomechanics and Biotribology in the Musculoskeletal System: Biomaterials and Tissues*. 2021.